Contributions to Mineralogy and Petrology (2020) 175:23
https://doi.org/10.1007/s00410-020-1660-9

ORIGINAL PAPER

Supersaturation Nucleation and Growth of Plagioclase: a numerical model of decompression-induced crystallization

Benjamin J. Andrews[1] · **Kenneth S. Befus**[2]

Received: 29 May 2019 / Accepted: 21 January 2020

Abstract

Supersaturation Nucleation and Growth of Plagioclase (SNGPlag) is a numerical model that predicts the nucleation and growth of plagioclase crystals in a decompressing magma as a function of time. The model is written in Matlab, but is available as a standalone compiled program. SNGPlag uses the MELTS webservice to determine equilibrium plagioclase mode, for a user-defined magma composition, as a function of pressure and temperature. User inputs include decompression path, the presence and size distributions of antecrysts and phenocrysts, and crystal shape. At each time step, the model evaluates the difference between the calculated crystallinity and equilibrium crystallinity for a given pressure and temperature to determine the degree of supersaturation, which then sets plagioclase nucleation and growth rates. Growth rates are used to grow the existing crystals whereas nucleation adds new crystals. SNGPlag produces results that can be compared to quantitative textures in natural volcanic rocks, including total crystallinity, microlite number density, microlite crystal size distribution, the characteristic size of microlite crystals, as well as a time series of crystallinity. Model results are consistent with the established crystallization theory. As expected, microlite crystallinity increases as decompression rate slows. Decompression path greatly affects microlite textures. For the same average decompression rate, single-step paths have higher crystallinities and microlite number densities than multi-step decompressions, which are in turn more crystalline than continuous paths. Pre-existing crystals damp microlite crystallization, as these crystals provide a substrate to accommodate crystal growth and thus reduce supersaturation. The size distribution and volume fraction of these pre-existing crystals determines the magnitude of the damping. SNGPlag predicts that melt composition and temperature also exert important controls. Higher temperatures and higher silica contents both reduce microlite crystallization. In comparison with the previous studies of decompression rate based on microlite crystallization experiments, SNGPlag generally predicts minimum decompression rates that are up to three-to-four times slower. The difference is likely because those studies applied single- or multi-step decompression experiments to simulate natural magma ascent, which may be better represented by continuous decompression pathways or series of continuous decompression intervals punctuated with pauses. Previous studies also fail to account for the effects of phenocrysts or antecrysts on microlite nucleation and growth.

Keywords Magma decompression · Crystallization kinetics · Plagioclase · Decompression rate · Ascent rate · Crystal size distribution

Communicated by Mark S Ghiorso.

Electronic supplementary material The online version of this article (https://doi.org/10.1007/s00410-020-1660-9) contains supplementary material, which is available to authorized users.

✉ Benjamin J. Andrews
andrewsb@si.edu

[1] Global Volcanism Program, Smithsonian Institution, Washington, DC 20560, USA

[2] Department of Geosciences, Baylor University, Waco, TX 76798, USA

Introduction

Magma decompression rate critically affects eruption behavior. Slow decompression allows exsolved volatiles to decouple from the magma, resulting in effusive eruption of lavas. Exsolved volatiles remain coupled to magma during fast decompression, leading to explosive eruption (e.g., Eichelberger et al. 1986; Jaupart and Allegre 1991; Yoshida and Koyaguchi 1999; Burgisser and Gardner 2005). When used with other parameters such as eruption rate or volume, decompression rates can be used to estimate conduit size or

Published online: 17 February 2020

eruption duration (e.g., Rutherford and Hill 1993; Andrews and Gardner 2010; Andrews 2014). Determining the likely rates of magma decompression and ascent is also very important for eruption forecasting as it provides an estimate of how fast an eruption might occur, and whether or not such an eruption might be explosive (NAS 2017).

Seismic records showing pre- or syn-eruption magma decompression exist for only a limited number of eruptions (e.g., Eaton et al. 1987; Swanson et al. 1987; Harlow et al. 1996; Power et al. 1996). Consequently, alternative methods of estimating decompression rate are required for unmonitored volcanoes, geophysically quiet systems, or prehistoric events. During eruption, magmas undergo significant changes in pressure–temperature conditions, resulting in volatile supersaturation and thermodynamic disequilibrium. Multiple decompression "speedometers" have been developed over the past decades that utilize the disequilibrium responses of crystals and melts to changes in those intensive parameters. Rocks provide the only record for the vast majority of eruptions, and thus, multiple techniques have been developed to estimate decompression rate. The most commonly used methods are analysis of crystal size distributions (e.g., Cashman 1988; Cashman and Marsh 1988; Marsh 1988; Suzuki and Fujii 2010; Mujin et al. 2017), bubble size distributions (Toramaru 2006), decompression experiments (e.g., Geschwind and Rutherford 1995; Hammer and Rutherford 2002; Couch et al. 2003; Martel and Schmidt 2003; Hammer 2004; Szramek et al. 2006; Suzuki et al. 2007; Castro and Dingwell 2009; Andrews and Gardner 2010; Brugger and Hammer 2010; Mollard et al. 2012; Shea and Hammer 2013; Waters et al. 2015; Befus and Andrews 2018), analysis of mineral reaction rims (e.g., Rutherford and Hill 1993; Devine et al. 1997; Browne and Gardner 2006), and diffusion profiling of melt embayments (e.g., Liu et al. 2007; Humphreys et al. 2008; Lloyd et al. 2014; Ferguson et al. 2016; Myers et al. 2016; Myers et al. 2018; Moussallam et al. 2019). All of those techniques rely on the difference between the rate at which the magma is forced into disequilibrium and the rate at which it can return to equilibrium through nucleation and growth of new crystals, reaction of existing crystals, or diffusion and vesiculation of volatile species. Decompression rates can vary over many orders of magnitude, from < 0.2 to > 30 MPa h^{-1} as estimated from microlite populations or mineral reaction rims, to rates > 1000 MPa h^{-1} as suggested by melt embayments. The response rates of the various decompression speedometers also vary over several orders of magnitude. Furthermore, the conditions required for application of a particular technique are not always present (e.g., presence of crystals, reaction rims, or melt embayments), and thus, not all techniques are applicable to all eruptions.

Of the different petrological approaches to estimating decompression rate, microlite textures interpreted through the lens of decompression experiments have broad applicability as microlites are present in many magmas. To build upon previous experimental and analytical works, we present a numerical model ("Supersaturation Nucleation and Growth of Plagioclase", SNGPlag) for predicting the plagioclase crystal populations that evolve during decompression of dacite and rhyolite magmas. We show that measured crystallinity, crystal size distribution, and crystal number densities can be used to infer the decompression rate of a range of explosive and effusive eruptions. Faster decompression rates tend to produce fewer microlites and smaller microlites than slow decompression rates. Notably, decompression path (i.e., single-, multi-step, or continuous; accelerating or decelerating; paused) and populations of antecrysts or phenocrysts in the magma at the initiation of decompression strongly affect the final microlite textures.

Background on crystal textures and magma ascent

Decompression experiments have been used to quantitatively estimate the decompression rates of several eruptions (e.g., Geschwind and Rutherford 1995; Coombs et al. 2002; Hammer and Rutherford 2002; Couch et al. 2003; Hammer 2004; Castro and Dingwell 2009; Andrews and Gardner 2010; Brugger and Hammer 2010; Martel 2012; Shea and Hammer 2013; Waters et al. 2015; Befus and Andrews 2018). To perform those experiments, workers decompress aliquots of magma from initial "pre-eruptive" conditions to some final pressure. The magma crystallizes in response to the imposed disequilibrium, through additional growth on phenocrysts or antecrysts, and/or nucleation and growth of new crystals. By running experiments at different decompression rates and comparing the end products with samples from the natural eruption of interest, workers can constrain the decompression rate of that eruption, and more broadly describe crystal nucleation and growth kinetics. Toramaru et al. (2008) use decompression-induced crystallization of microlites to develop a rate meter for water exsolution based on microlite number densities.

Experimental studies provide the only controlled measurements of crystal nucleation and growth, and thus, they are the basis for all quantitative studies of how crystal populations evolve in response to changes in intensive parameters. Importantly, and not surprisingly, the experimental results are highly dependent upon experimental setup, including the type of starting material and the decompression path (e.g., single-step, multi-step, or continuous). Most experimental studies have used single- or multi-step decompression paths. Continuous decompression studies by Brugger and Hammer (2010), Martel (2012), Befus et al. (2015), Waters et al. (2015), and Befus and Andrews

(2018) have shown that decompression path, not just rate, greatly influences the final texture. Many experimental studies have focused on plagioclase because of its ubiquity in volcanic rocks and its common occurrence as a microlite phase. For the purposes of this paper, we will define antecrysts as crystals that have not grown from the magma in which they reside, phenocrysts as crystals that have grown from and are present in the magma prior to decompression and ascent, and microlites as crystals that nucleate and grow during decompression and ascent (and potentially during cooling).

Crystal size distributions (CSDs) have been recognized as preserving a record of magma decompression (and cooling) for many years. Seminal papers by Marsh (1988) and Cashman and Marsh (1988) describe how a magma should nucleate and grow crystals in response to thermodynamic disequilibrium, and how the size distribution of those crystals should evolve through time. CSDs are potentially powerful records of magma disequilibrium as they provide an integrated record of magma history between storage and eruption. The two primary parameters controlling the evolution of any CSD are the crystal nucleation and growth rates, such that a log-linear cumulative population distribution will evolve through time for constant nucleation and growth rates; we note, however, that nucleation and growth rates should not necessarily be constant. CSDs that show a change in slope are thus interpreted to record a change in nucleation and/or growth rates, which is in turn interpreted to reflect a change (or stop) in decompression (or cooling) rate. The analytical techniques described in these papers have been used to infer decompression paths or to describe nucleation and growth rates (Cashman 1988; Hammer et al. 1999; Brugger and Hammer 2010; Suzuki and Fujii 2010; Mujin et al. 2017). Because of its ubiquity in volcanic rocks and common occurrence as a microlite phase, most studies have focused on plagioclase, although, in principle, this technique should be applicable to any mineral phase. Importantly, CSDs do not unambiguously describe decompression, nucleation, or growth rates. Estimating decompression rate from CSDs requires independent knowledge of nucleation and growth rates (and assumption that those rates are constant), and, conversely, estimating assumed constant nucleation and growth rates requires independent knowledge of total time available for crystallization.

The many previous studies of experimental and natural samples demonstrate the utility of analyzing microlite textures (including CSDs) to elucidate decompression paths. Those studies also show that many factors affect the manner in which crystal populations evolve. Thus, there is need for a universal model that can predict crystallization during decompression and be used to estimate the decompression rates recorded by crystal populations in natural samples.

Model equations and methodology

Supersaturation Nucleation and Growth of Plagioclase ("SNGPlag") is an isothermal, iterative model that calculates the evolution of a plagioclase crystal population in 1 m^3 of magma with user-specified composition through a specified pressure–time path. The model is written in Matlab and then compiled into a standalone executable program using the Matlab Compiler and Matlab Runtime. The program can be downloaded from VHub (https://vhub.org/resources/4524).

Decompression or cooling of a melt will increase its degree of supersaturation, $\Delta\phi$. Nucleation and growth of crystals in response to that increase supersaturation will act to return the magma to equilibrium (Fig. 1). At each time step, plagioclase supersaturation, $\Delta\phi_{plag}$, is calculated using the MELTS web service (Gualda et al. 2012; Ghiorso and Gualda 2015) and then used to determine the instantaneous nucleation and growth rates of plagioclase (Befus and Andrews 2018). Those rates are then applied to grow the existing crystals and nucleate new crystals. The model outputs plagioclase crystallinity and supersaturation through time, CSD, number density, and characteristic microlite size. The model thus allows for rapid comparison with textures in natural or experimental samples. Unlike previous models of microlite nucleation and growth, SNGPlag does not assume a single nucleation rate, but instead allows nucleation and growth to be path dependent.

Model runs require an input file describing the plagioclase liquidus and the plagioclase volume fraction as a function of pressure and temperature. Such files are generated through upload of a file containing the magma composition. Ideally, this is the bulk composition of melt and phenocrysts, which is approximated by melt composition for crystal-poor

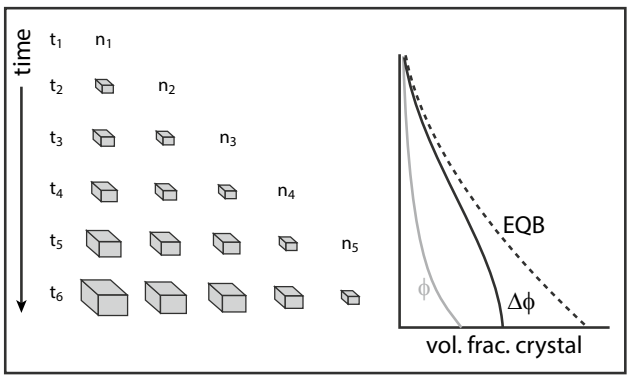

Fig. 1 Schematic of SNGPlag model. At time t_x, n_x crystals nucleate (where "x" is time steps 0, 1, 2, 3, etc.). At time t_{x+1}, growth occurs on all crystals present in the previous time step, and n_{x+1} new crystals nucleate. Crystallinity ϕ at any time is the sum of all crystal volumes at that time. The supersaturation, $\Delta\phi$, as a function of time is defined as the difference between the equilibrium crystallinity (EQB) and ϕ

magmas. We note, however, that many magmas of interest contain large fractions of phenocrysts and antecrysts, and their residual melt compositions may not be the best input parameters; for such magmas, the ideal input composition is instead the bulk composition minus the contribution of antecrysts. After an input file is loaded, the program calls the MELTS webservice to find liquidus surfaces and the plagioclase fractions, ϕ_{eqb}, throughout pressure–temperature space as defined by the user. We use the MELTS version "rhyolite-MELTS 1.0.2," which is optimized for hydrous silicic magmas, but can be applied to the same range of compositions as MELTS, with the caveat that it is not suitable for intermediate composition magmas with abundant by biotite or hornblende (Gualda et al. 2012; Ghiorso and Gualda 2015). In addition to generating an input file for subsequent decompression runs, the program saves all of the MELTS output files in .xml format.

To run the model, the user first loads the MELTS input file. The program then requests the user input the following variables: initial and final pressure (P_{init}, P_{final}), initial temperature (T_{init}), decompression rate (dP/dt), decompression path, crystal geometry, and the volume fraction and size distributions of phenocrysts and/or antecrysts. SNGPlag works for any decompression rate. The decompression path can be either continuous, single-step, or multi-step (Fig. 2). For multi-step decompressions, the user must define the number of equal-pressure steps through which the magma decompresses. Continuous decompression rates will typically be linear, although we allow the user to add a pause of specified duration at a specified pressure to simulate magma stalling. Furthermore, accelerating or decelerating pathways can also be selected (Fig. 2). The software can run multiple decompression models using

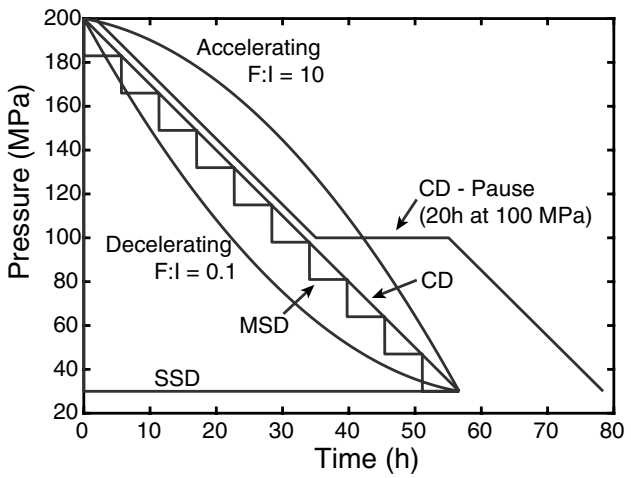

Fig. 2 Example decompression paths for continuous (CD), single-step (SSD), multi-step (MSD), accelerating, decelerating, and paused decompressions. Note that the average rate for all paths, except the paused run, is the same

different conditions in series, but we will first discuss a single run.

All crystals are modeled as rectangular prisms. During growth, crystal proportions remain constant regardless of crystal size (i.e., a tabular crystal with dimensions of $1 \times 0.5 \times 0.25$ grows with rates proportional to each axis and thus preserves its geometry). Phenocrysts and antecrysts are together grouped as the crystals existing prior to the start of decompression. Microlites are juvenile crystals that nucleate in response to supersaturation. The phenocryst volume fraction is generated using the phase equilibrium as calculated by MELTS (Gualda et al. 2012; Ghiorso and Gualda 2015). In contrast, the presence of antecrysts does not initially affect the thermodynamic equilibrium of the magma. Thus, a magma above the plagioclase liquidus can contain plagioclase antecrysts but not phenocrysts. For modeling purposes, phenocrysts can be excluded from runs that initiate below the plagioclase liquidus.

SNGPlag calculates the P–T–t path of the magma over a series of 5000 time steps with duration Δt. SNGPlag then uses that path and the MELTS-generated phase equilibria to determine the equilibrium plagioclase volume fraction as a function of time. The initial crystal population is defined by the population of phenocrysts and antecrysts, but only the initial volume fraction of phenocrysts applies toward the plagioclase crystallinity. At each time (t_i), the instantaneous disequilibrium ($\Delta\phi_{plag}$) is calculated as the difference between the equilibrium plagioclase volume fraction (ϕ_{eqb}) and the calculated plagioclase crystallinity (ϕ_{plag}) at time t_{i-1}. That $\Delta\phi_{plag}$ value is then used to determine the instantaneous nucleation and growth rates, $I(t)$ and $G(t)$, respectively. Growth on existing crystals is determined by increasing the size of each crystal by $G(t)*\Delta t$, proportional to each crystal dimension. All new crystal growth applies towards calculation of the plagioclase crystallinity, whether it is on "new" or existing microlites, phenocrysts, or antecrysts. New microlite crystals are added to the system in an amount equal to $I(t)*\Delta t$; these new crystals have an initial size of zero, but can accommodate growth in the next time step.

SNGPlag accounts for volume interferences between crystals (two crystals cannot occupy the same space) through a parameterized and probabilistic approach. Although trivial at low concentrations, volume interferences between crystals become noticeable as crystallinity rises. Assuming that the characteristic crystal size is small relative to the total system volume, which is true given 12 orders of magnitude difference between the volumes of a 100 μm crystal and the modeled space, then the amount of volume interference, ϕ_{int}, for a randomly distributed population of crystals can be calculated as:

$$\phi_{\text{int}} = 0.5\left(\phi_{\text{app}}\right)^2, \tag{1}$$

where ϕ_{app} is the apparent crystallinity (e.g., calculated with crystal overlap allowed). This in turn results in the expression:

$$\phi_{\text{plag}} = \phi_{\text{app}} - \phi_{\text{int}}, \tag{2}$$

that gives crystallinity, ϕ_{plag}, with overlapping crystals removed. This equation yields a smoothly varying curve of expected volume interference as a function of calculated crystallinity (Fig. 3).

At the end of each run, SNGPlag saves all of the output calculations, including time-dependent pressure, temperature, ϕ_{eqb}, ϕ_{plag}, $\Delta\phi_{\text{plag}}$, and crystal populations. The program automatically generates plots of several of those parameters, including the final CSD (Fig. 4); all CSDs exclude crystals smaller than 0.1 μm. N_v is presented for crystals larger than 0.1 μm and 1 μm; those minimum sizes are selected as proxies for crystal size detection limits in measurements of natural samples (e.g., detection limits of 0.1 μm or 1 μm respectively). SNGPlag provides an estimate of the uncertainty in N_v based on N_v and the characteristic crystal size, Sn. This Sn is the size at the 50% value of the cumulative size distribution. The uncertainty in N_v, σ_{Nv}, is determined with the equation:

$$\sigma_{\text{Nv}} = \left(\text{Sn}N_v\right)^{-1/2}, \tag{3}$$

which applies counting statistics to the probability of intersecting a crystal of size Sn (determined from the 50 percentile of the CSD) in a 1 mm^2 area. For single runs, SNGPlag generates a 3D visualization of the modeled crystal population (Fig. 5). A pseudo thin-section view of the modeled rock can be made by limiting the z-range of this visualization to 30 μm (Fig. 5).

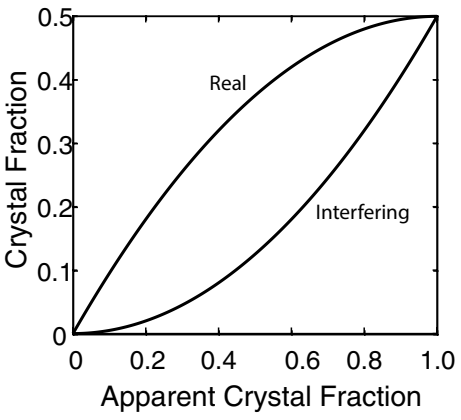

Fig. 3 Real and interfering crystal fractions, ϕ_{plag} and ϕ_{int}, respectively, as functions of apparent crystallinity, ϕ_{app}. Note that $\phi_{\text{plag}} = \phi_{\text{app}} - \phi_{\text{int}}$

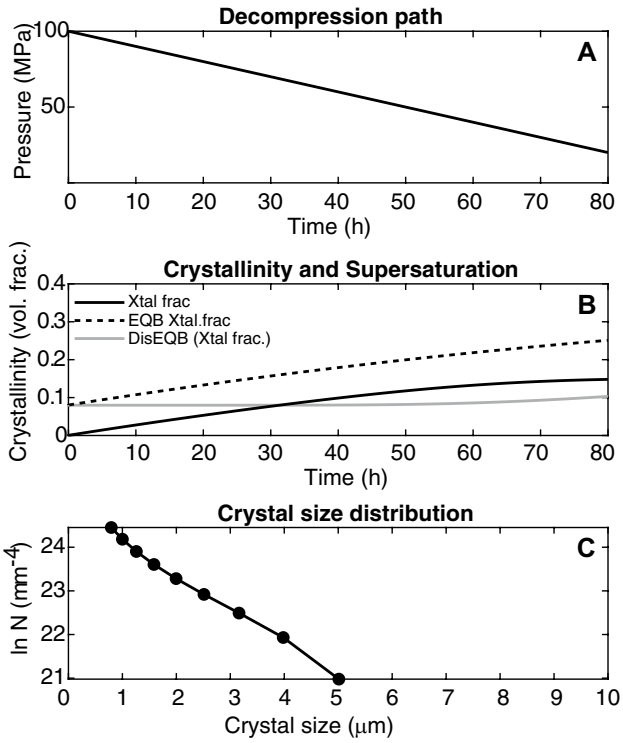

Fig. 4 SNGPlag model output for a single run decompressed from 100 to 30 MPa. **a** Decompression path. **b** Time series describing crystallinity (Crystal frac.), equilibrium crystal fraction (EQB crystal frac.), and supersaturation (DisEQB). **c** Crystal size distribution

If multiple decompression scenarios are run in series, each run proceeds in the same manner as described above, with all output calculations saved, but a different set of final plots is generated. No 3D visualization is generated; instead, SNGPlag produces a series of comparative plots showing variation in plagioclase crystallinity, N_v, and crystal size as functions of decompression rate, and a single diagram with all CSDs plotted (Fig. 6). For the final outputs, only crystals longer than 0.1 μm are counted in the CSDs, and N_v with minimum sizes of 0.1 μm and 1 μm are reported. We note that all of these parameters (crystallinity, N_v, CSD, and Sn) are commonly measured, thus natural samples can be easily compared to the SNGPlag calculations.

Choice of nucleation and growth rates

Many previous experimental studies have presented average or integrated crystal nucleation and growth rates (e.g., Hammer and Rutherford 2002; Couch et al. 2003; Brugger and Hammer 2010; Shea and Hammer 2013). Those rates are often presented as functions of undercooling (ΔT), which is the isobaric difference between the experiment temperature and the liquidus temperature of the phase of interest.

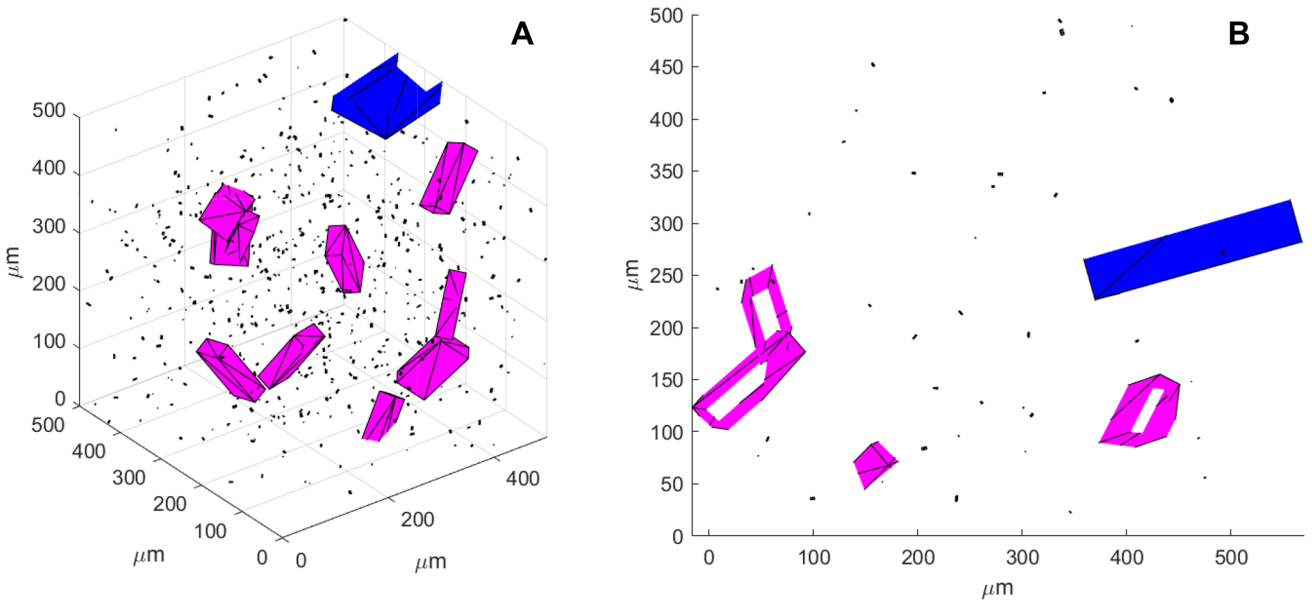

Fig. 5 **a** 3D rendering of SNGPlag model outputs for run shown in Fig. 4. Antecrysts (blue), phenocrysts (magenta), and microlites (small, green/black). **b** Pseudo-thin-section rendering of a 30 μm slice from panel **a**. The white areas within the magenta phenocrysts are artifacts of the manner in which the program renders crystals as hollow boxes

ΔT is used as a proxy for thermodynamic disequilibrium, with the implicit or explicit understanding that the value of ΔT changes as a system crystallizes. Unfortunately, measuring the change in ΔT through time is elusive, and thus, the maximum value of ΔT (ΔT_{max}) is used to characterize any particular rate.

Befus and Andrews (2018) show that supersaturation, $\Delta\phi$, for any particular phase can instead be quantified as the difference between the equilibrium and actual crystal fraction of the phase of interest at given pressure–temperature conditions. For example, if a magma has 3 vol% plagioclase, but the equilibrium plagioclase crystallinity is 10 vol% at that pressure and temperature, it has $\Delta\phi_{plag} = 0.07$. Furthermore, they show that the instantaneous plagioclase nucleation and growth rates, as functions of $\Delta\phi_{plag}$, have a different functional form and are ~ 50 times larger than the time-averaged values presented in Hammer and Rutherford (2002). Previous workers have described activation energies required for nucleation as well as nucleation lag or incubation times (e.g., Turnbull 1948; Nabelek et al. 1978; Couch et al. 2003). Although the Befus and Andrews (2018) nucleation rates do not explicitly have an activation energy nor lag time, those factors are implicit as the nucleation rate is effectively zero for $\Delta\phi \leq 0.04$.

The SNGPlag model uses the nucleation and growth rates from Befus and Andrews (2018) by default. The rates from Hammer and Rutherford (2002) can also be selected by the user. Table 1 compares the effects of the different nucleation and growth rates on N_v and sample crystallinity as applied to the 1991 Pinatubo dacite.

Compositional range

The modeling approach used by SNGPlag should be appropriate for all compositions of magma, but instantaneous nucleation and growth curves are only available for the Pinatubo dacite magma with rhyolitic melt (Befus and Andrews 2018). Consequently, at this time, SNGPlag is best calibrated for systems with rhyolitic melt composition (e.g., bulk rock equivalent to rhyolites, dacites, and crystal-rich andesites). Future work describing instantaneous nucleation and growth rates is required to optimize SNGPlag for magmas of other compositions and over a broader range of temperature. With that qualification, the model will run on any magma composition input by the user. Briefly, the plagioclase liquidus will be shifted to higher P–T conditions and ϕ_{eqb} at any given pressure and temperature will be higher in more mafic magmas; the effects of these changes are discussed in more detail below.

Generalized model results

SNGPlag predicts significant and systematic differences in microlite CSDs, N_v, and bulk crystallinity as decompression rate, path, temperature, and antecryst or phenocryst populations are varied. Here, we summarize model results over a broad range of parameter space as calculated for the white Ksudach KS1 rhyodacite (Table 2) (Andrews et al. 2007; Andrews and Gardner 2010). Initial conditions for all runs are presented in Supplementary Material 1.

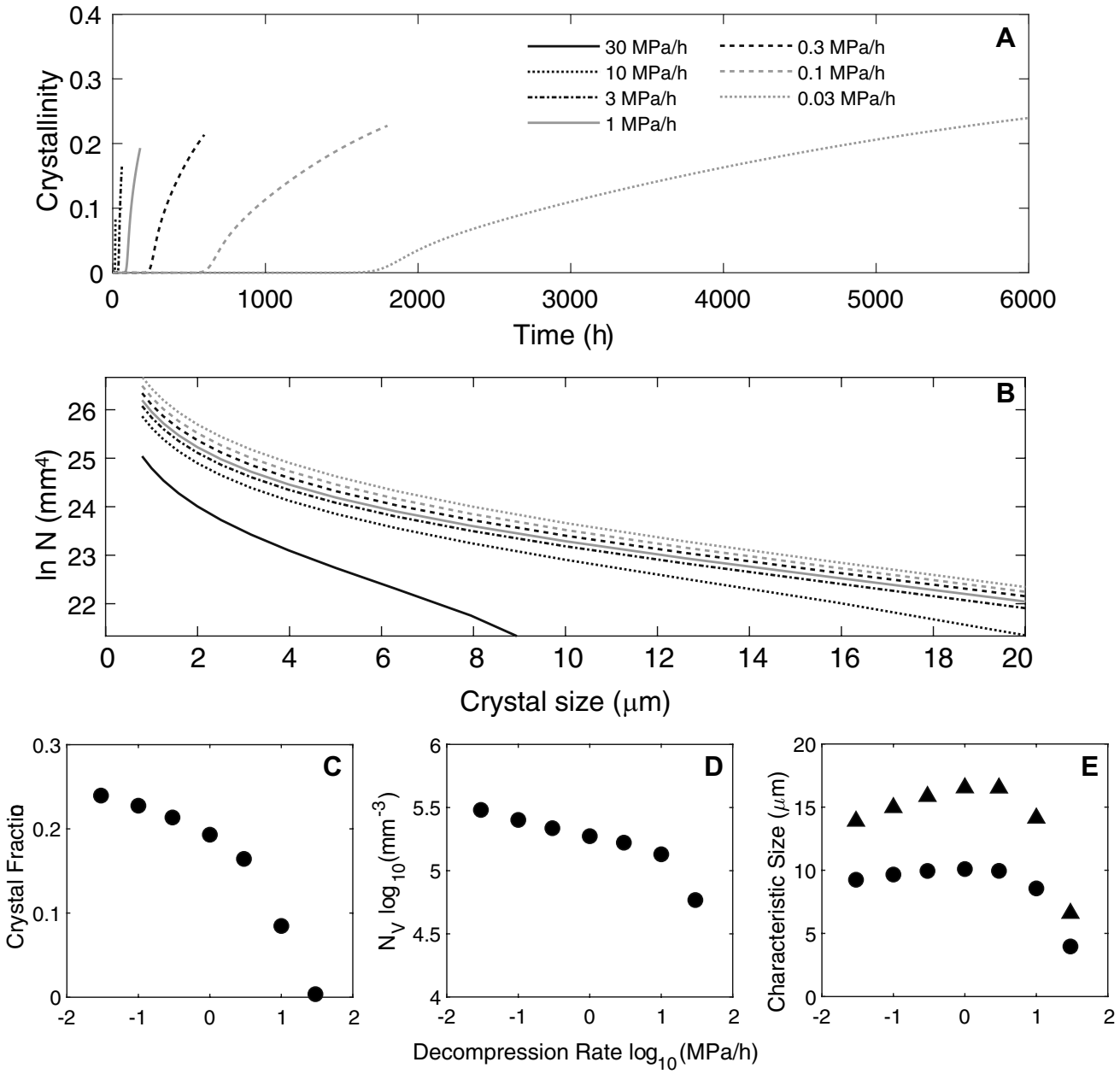

Fig. 6 SNGPlag outputs for variation in steady (linear) decompression rate. **a** Sample crystallinity through time. **b** Final sample CSDs. **c** Final crystal fraction. **d** Final number density, N_v (larger than 1 μm). **e** Characteristic size, Sn (triangles = 50 percentile; circles = equant method)

Table 1 Comparison of SNGPlag results using Befus and Andrews (2018) and Hammer and Rutherford (2002) nucleation and growth rates

Run		Growth rates	Crystallinity	Nv (mm^{-3})	Nv1 (mm^{-3})	CSD50 (m)	S50 (m)	Sn (m)
RateComp-1	CD	BA	0.23537122	251564.15	240942.61	1.5849E−05	1.4E−05	9.51E−06
RateComp-2	CD	HR	0.02852524	1077.806	0	1.9953E−07	0	0
RateComp-3	SSD	BA	0.25881848	204602.42	189517.915	1.5849E−05	1.54E−05	1.07E−05
RateComp-4	SSD	HR	0.02869441	2128.7875	0	2.5119E−07	0	0

All runs conducted using Pinatubo composition (Table 2), $T = 780$ °C, $P_{init} = 220$ MPa, $P_{final} = 30$ MPa, and average decompression rate of 0.1 MPa/h. Crystal shape 1 × 0.5 × 0.25; no antecrysts/phenocrysts

Table 2 Compositions used in model runs

Eruption	References	SiO2	TiO2	Al2O3	Fe2O3	Cr2O3	FeO	MnO	MgO	NiO	CoO	CaO	Na2O	K2O	P2O5	Total
Pinatubo 1991	Befus and Andrews (2018)	77.0	0.11	13.46	0	0	1.08	0.06	0.21	0	0	1.61	3.55	2.94	0	100.02
Ksudach KS1	Andrews and Gardner (2010)	71.48	0.45	14.54	0.00	0.00	3.14	0.14	0.78	0.00	0.00	2.84	5.18	1.37	0.00	99.92
Augustine WR 2006	Coombs and Vazquez (2014)	62.37	0.56	16.77	0.00	0.00	5.28	0.12	3.23	0.00	0.00	6.70	3.84	1.00	0.13	100.00
Augustine MG 1986	Roman et al. (2006)	75.8	0.35	12.62	0	0	1.69	0	0.38	0	0	1.66	4.23	2.23	0	98.96
Chaiten 2008	Castro and Dingwell (2009)	76.10	0.13	13.70	1.27	0.00	0.00	0.06	0.28	0.00	0.00	1.41	4.00	2.98	0.04	99.97
Santa Maria 1902	Andrews (2014)	66.80	0.31	16.60	1.24	0.00	2.30	0.16	1.15	0.00	0.00	3.63	4.99	1.88	0.19	99.25
Mount St. Helens 1980	Rutherford et al. (1985)	62.81	0.60	17.89	0.00	0.00	3.91	0.07	1.70	0.00	0.00	5.29	4.88	1.29	0.00	98.44

All runs initiated with 10 wt% H_2O (water saturated). Oxygen fugacity for all runs set at log f_{O2} = NNO + 1

Microlite crystallinity varies systematically with decompression rate for model runs decompressed from 200 to 20 MPa at 850 °C using a series of different linear, continuous rates (Fig. 6). Each simulation contains no antecrysts and, as the runs begin above the plagioclase liquidus, they contain no phenocrysts. As decompression rate decreases from 30 to 10 to < 1 MPa h^{-1}, crystallinity increases from < 1 to 8.5 to ≥ 20 vol% (Fig. 6a, c). At the slowest investigated rate, 0.03 MPa h^{-1}, the magma achieves 24 vol% crystallinity, but does not reach the equilibrium crystallinity of ~ 30 vol%. Similarly, microlite number density responds to the different decompression rates. The fastest decompression of 30 MPa h^{-1} produces a number density of ~ 6×10^4 mm^{-3}, which increases to ~ 1.4×10^5 mm^{-3} at 10 MPa h^{-1}, ~ 1.8×10^5 mm^{-3} at 1 MPa h^{-1}, and finally to ~ 3×10^5 mm^{-3} at 0.03 MPa h^{-1} (Fig. 6d). N_v decreases approximately linearly with the log of decompression rate (Fig. 6e). The characteristic crystal size shows a different pattern, with size increasing from ~ 6 to ~ 20 µm as decompression rate decreases to 3 MPa h^{-1}, but then decreasing to ~ 15 µm at slower decompression rates. The CSDs systematically vary with decompression rate (Fig. 6b): fast decompression produces lower amplitude, more steeply sloped CSDs than slower decompression.

Decompression path affects sample crystallinity, particularly for faster average decompression rates as there is less total time available for the system to equilibrate (Fig. 7). The SSD runs show much greater crystallinity than MSD or continuous runs (Fig. 7b). Microlite N_v is highest in the SSD simulations, but the effect diminishes at slower decompression rates (Fig. 7c). At fast decompression rates the characteristic size is largest for SSD runs (~ 16 µm) followed by MSD simulations (~ 8 µm), and then continuous runs (~ 6 µm); whereas at slow rates, there is no substantial difference between the characteristic sizes (Fig. 7c, d).

Accelerating or decelerating decompression paths result in textures that strongly reflect the late stage decompression rates (Fig. 7). Because overall crystallization rates are greatest at high values of supersaturation, $\Delta\phi_{plag}$, and those values are most likely to be achieved at lower pressures, accelerating rates have the effect of rapidly transiting the pressures where high $\Delta\phi_{plag}$ should be expected. Consequently, accelerating paths crystallize fewer and smaller crystals than constant rate paths (Fig. 6). Decelerating paths, in contrast, show textures that are intermediate between constant rate and SSD runs (Fig. 7); this is not surprising given that a very low final:initial decompression ratio would approximate a SSD path.

Sometimes magmas stall during conduit ascent (e.g., Cashman 1988; Berlo et al. 2004; Browne and Gardner 2006). SNGPlag simulates this process through the introduction of a pause during a continuous decompression run. The pause affects the resulting microlite textures, but

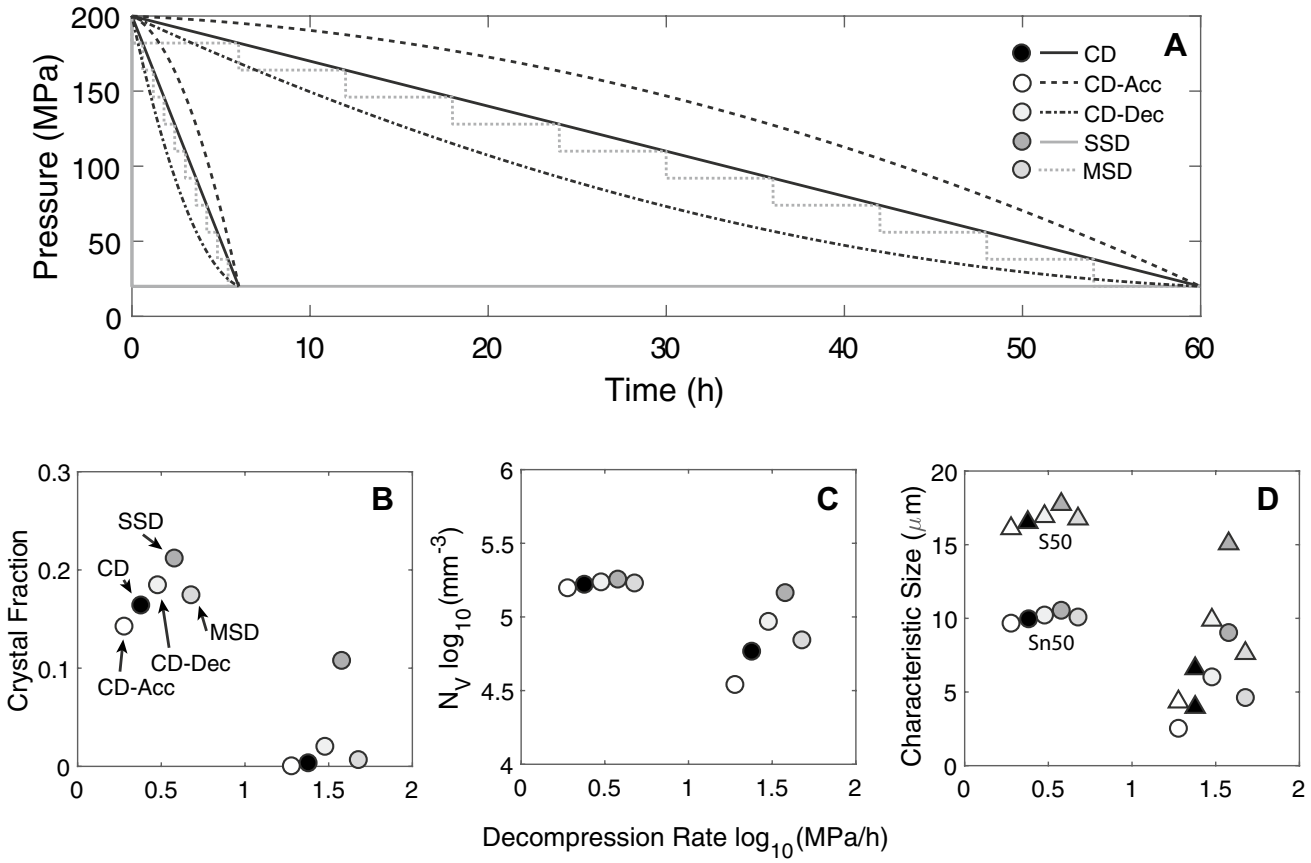

Fig. 7 Effects of decompression path. **a** Decompression path (*CD* continuous steady, *CD-Acc* continuous accelerating, *CD-Dec* continuous decelerating, *SSD* single-step, *MSD* multi-step). **b** Final crystal fraction. **c** Final N_v. **d** Final Sn (triangles = 50 percentile; circles = equant method). Symbols in panels **b**, **c**, and **d** have been offset from their average decompression rates to eliminate overlap

the pressure at which that pause occurs, and its duration, determine the magnitude of its effect (Fig. 8). Pauses at pressures just below the plagioclase liquidus have much less effect on final textures than pauses at lower pressures. For demonstration, continuous decompression of the KS1 rhyodacite from 200 to 20 MPa at 30 MPa h^{-1} produces a rock with ~ 0.3 vol% crystallinity with a characteristic size of ~ 6 µm plagioclase and a N_v of 6×10^4 mm^{-3}. Adding a pause of 12 h at 150 MPa increases the crystallinity to ~ 4 vol% and the characteristic size to ~ 8 µm, with N_v only slightly increasing. A much larger effect is produced with a pause at 50 MPa, which results in a final crystallinity of ~ 13 vol% microlite crystallinity with a characteristic size of ~ 16 µm and an N_v of ~ 1.5×10^5 mm^{-3}. The duration of the pause is similarly influential, with longer durations resulting in greater crystallization. The relative importance of pause duration is a function of decompression rate. Slower decompression rates are less effected by a pause than faster rates.

Crystal shape can also significantly affect microlite crystallinity, N_v, Sn, and CSDs. Crystal shape within SNGPlag controls the growth rates of the a, b, and c axes and the relative surface areas of each face. We examine the effects of crystal morphology on microlite textures by comparing four specific geometries: equant ($1 \times 1 \times 1$), planar ($1 \times 1 \times 0.25$), acicular ($1 \times 0.1 \times 0.1$), and tabular ($1 \times 0.5 \times 0.25$). We simulate crystallization of the different morphologies with decompressions from 200 to 20 MPa at 850 °C at 3 MPa h^{-1} (Fig. 9). Equant crystals produce the highest crystallinity (~ 18 vol%) and the lowest N_v (~ 10^5 mm^{-3}). Planar and tabular crystals produce the next highest crystallinities and lower N_v. Acicular crystals produce the lowest crystallinity (~ 13.5 vol%) and highest N_v (~ 3×10^5 mm^{-3}). Characteristic crystal size also depends on geometry. Using the method of Cashman (1988), equant crystals produce larger overall sizes than the other forms, but evaluation of size based on the length of the 50th percentile crystal shows that acicular crystals produce the longest crystals. This result is predictable given that determination of Sn based on the c-axis length (the 50th percentile method) will bias towards acicular geometry, whereas the volume-based method of Cashman (1988) will favor larger volume (equant) crystals.

The presence of phenocrysts or antecrysts strongly affects microlite nucleation and growth, and, consequently, the overall crystallization history of a magma, its final

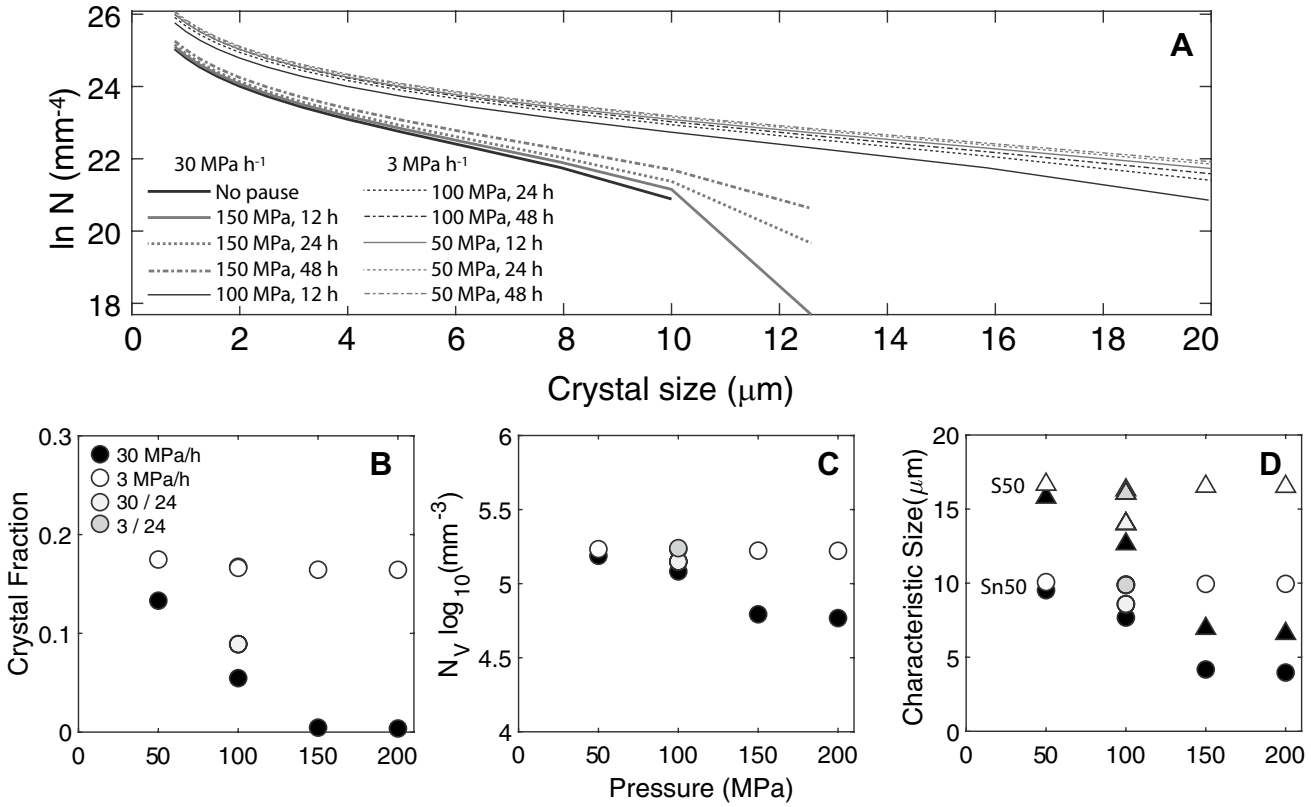

Fig. 8 Effects of 12 and 24 h pauses at 150, 100, and 50 MPa **a** CSDs. **b** Final crystal fraction. **c** Final N_v. **d** Final Sn (triangles = 50 percentile; circles = equant method)

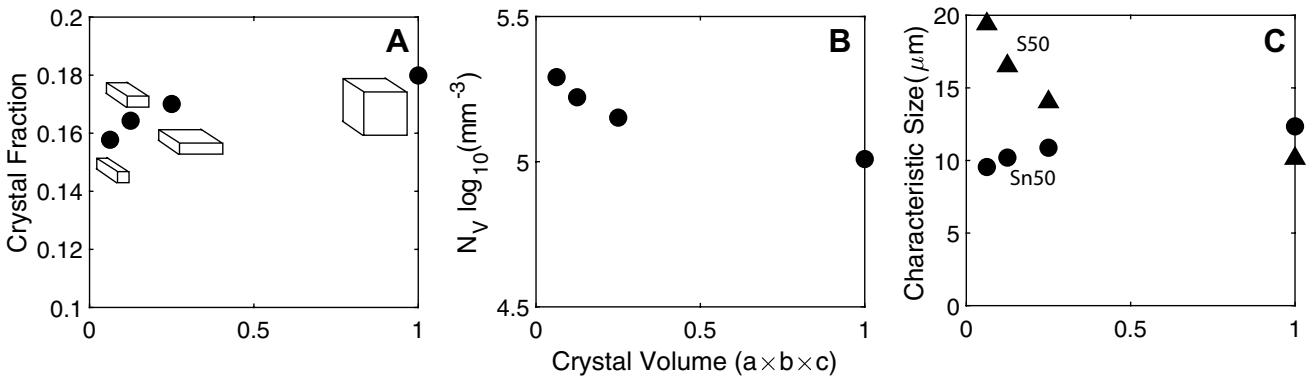

Fig. 9 Effects of crystal shape. **a** Final crystal fraction as a function of crystal unit volume; crystal shapes shown schematically. **b** Final N_v. **c** Final Sn (triangles = 50 percentile; circles = equant method)

crystallinity, N_v, and CSD. When antecrysts or phenocrysts are present, they provide a substrate to accommodate crystal growth without the need for nucleating new crystals. Hence, pre-existing crystals allow the system to more efficiently crystallize and never achieve as high of a degree of supersaturation, especially during the early stages of crystallization (Fig. 10a, b). Because nucleation rate increases with supersaturation, systems without pre-existing crystals are likely to nucleate more microlites, resulting in a higher final N_v (Fig. 10c) Interestingly, as decompression continues, more microlites will eventually produce samples with the highest crystal surface areas. Although an initially crystal-free magma may crystallize at a slower rate during the early stages of decompression, it can also finish with a higher crystallinity than an initially crystal-bearing magma (Fig. 10a, b).

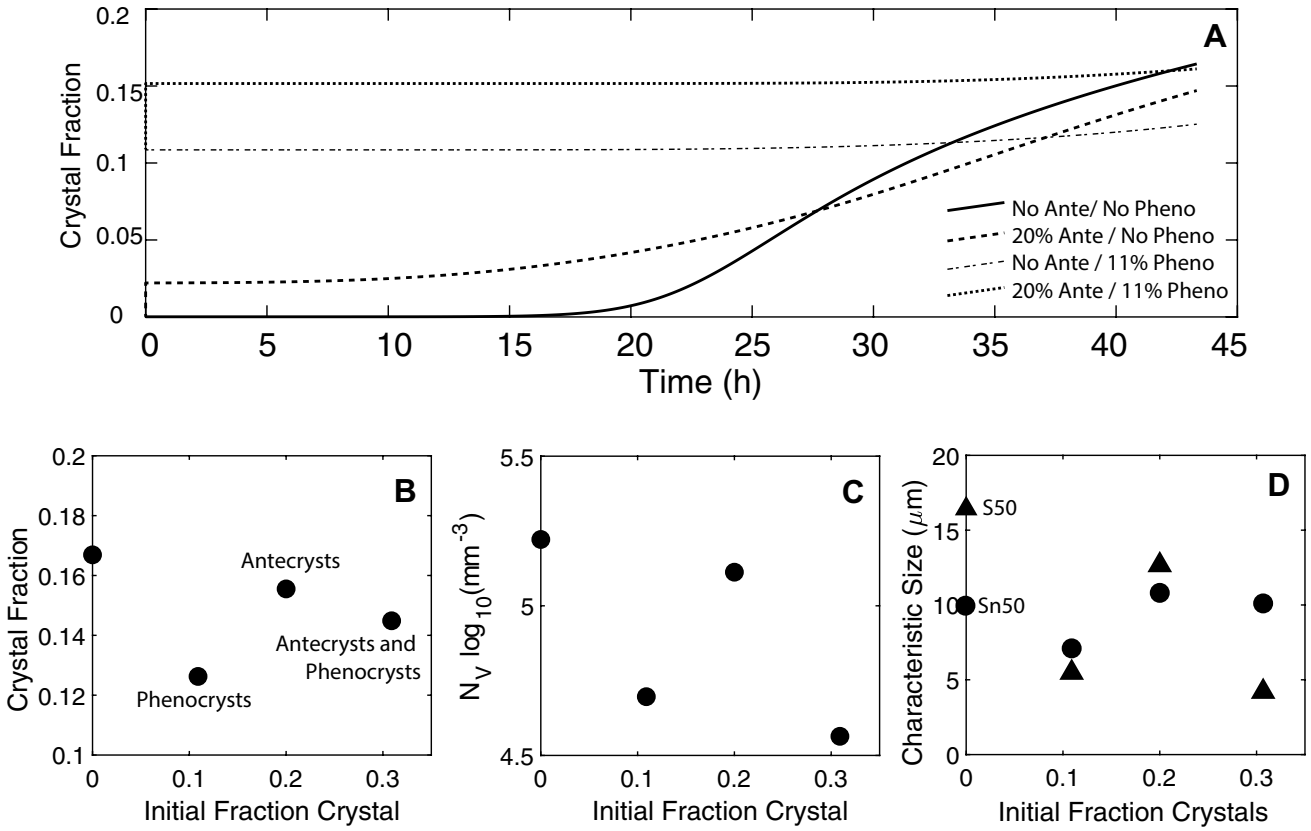

Fig. 10 Effects of antecrysts and phenocrysts. **a** Sample crystallinity through time. **b** Final crystal fraction. **c** Final N_v. **d** Final Sn (triangles = 50th percentile; circles = equant method). The initial 20 vol% antecrysts is an arbitrary value, whereas the initial 11 vol% phenocrysts is the equilibrium volume fraction plagioclase at the initial conditions of 150 MPa and 850 °C

The magnitude of the effects of antecrysts on decompression-induced crystallization is dependent on the total surface area of the crystals, rather than their volume fraction. As the total crystal surface area is a function of crystal volume fraction and size distribution, the same volume fraction antecrysts can have very different effects on microlite crystallization if the crystal sizes are different (Fig. 11). Assuming the same volume fraction, larger antecrysts produce lower crystallinities, higher microlite number densities, and larger characteristic sizes than smaller antecrysts; those effects are, however, complex, such that intermediate size distributions can have lower final crystallinities that fine or coarse distributions. Finally, it is possible for different antecryst volume fractions and size distributions to have the same effect on certain aspects of microlite crystallization; for example, 20 vol% 400 µm antecrysts will result in the same N_v as ~ 0.5 vol% 25 µm antecrysts. However, different antecryst populations will not simultaneously reproduce all characteristics of microlite crystallization (crystallinity, number density, and characteristic size).

Changes in temperature or magma composition also affect crystallization processes (Fig. 12). This is expected as both variables change the position of the liquidus and contours of equilibrium crystallinity with respect to the modeled decompression path. If composition and decompression rate are held constant, shifting to a lower temperature results in a higher final crystallinity and N_v, and an upward shift in the resulting CSD. Conversely, increasing temperature results in a decrease in crystallinity. Note, however, that the presence of phenocrysts can complicate those predictions, as they both reduce the initial supersaturation and provide a substrate for new growth. Because phenocrysts are allowed in the runs, and some of the runs initiate below the liquidus, the runs start with different crystallinity. As a consequence, although the coolest run finished with the highest crystallinity, the intermediate temperature run (850 °C) finishes with the highest N_v.

For a given temperature, increasingly mafic compositions should act in a manner analogous to lowering the temperature (e.g., increasing crystallinity) (Fig. 12). The 900 and 950 °C 2006 Augustine andesite runs provide an example of these effects, producing similar final crystallinities and N_v as the much cooler 800 and 850 °C Ksudach runs (Table 2; Coombs and Vazquez 2014). On the other hand, if the andesite is treated as a silicic melt containing a large fraction of antecrysts (e.g., 1986 Augustine rhyolite

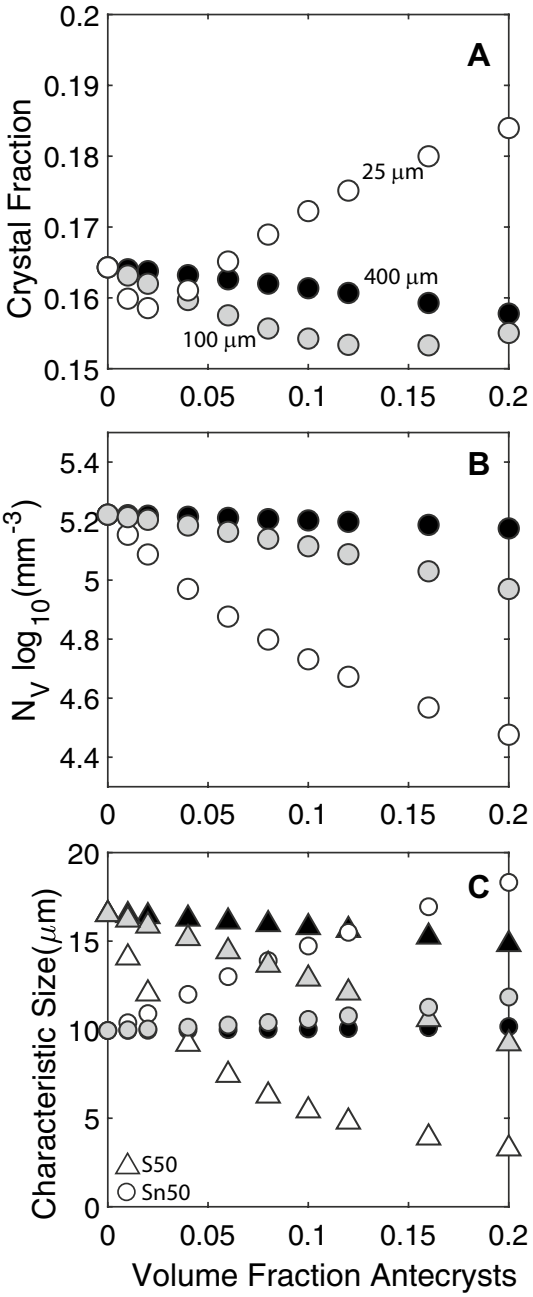

Fig. 11 Effects of initial antecryst fraction and size. **a** Final crystal fraction. **b** Final N_v. **c** Final Sn (triangles = 50 percentile; circles = equant method)

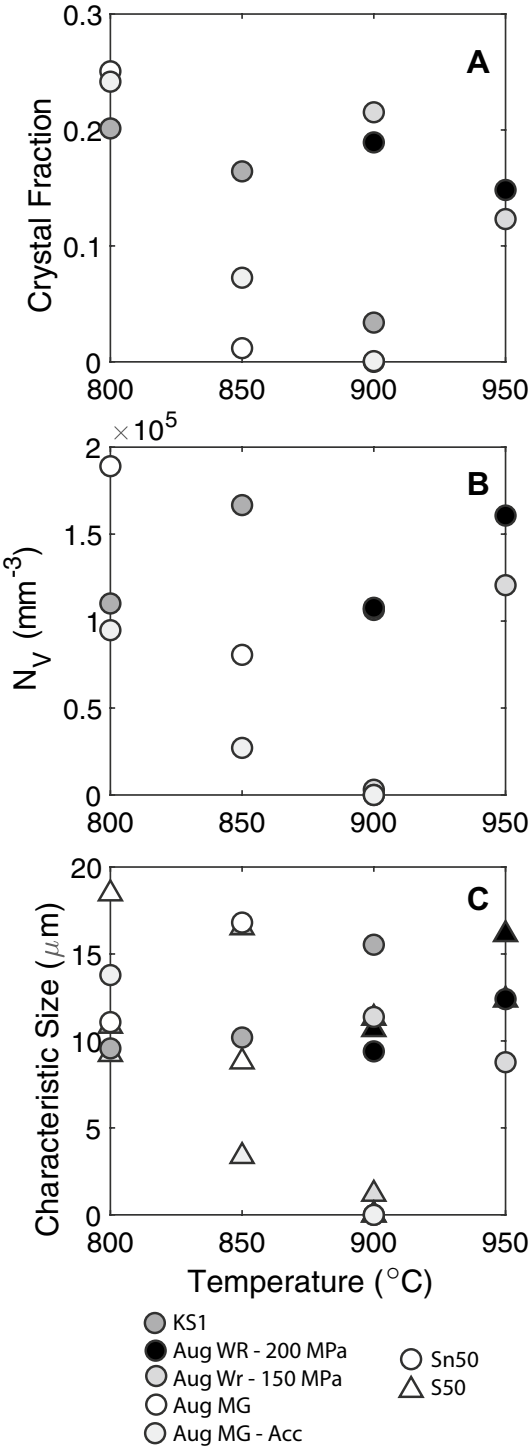

Fig. 12 Effects of temperature and composition. **a** Final crystal fraction. **b** Final N_v. **c** Final Sn (triangles = 50 percentile; circles = equant method)

matrix glass with ~ 30 vol% antecrysts, Roman et al. 2006), then the "bulk andesite" system displays behavior more similar to that of the rhyodacite. For example, at 800 °C, the "bulk andesite" system has a final crystallinity of 24 vol% and N_v of 1.1×10^5 mm^{-3} as compared to 20 vol% and 9.5×10^4 mm^{-3} for the rhyodacite. This demonstrates ways in which SNGPlag can be applied to whole rock compositions even in crystal-rich magmas.

Uniqueness of solutions

Crystallinity, N_v, and CSDs all change in response to temperature, pressure, the presence and size distributions of

antecrysts and/or phenocrysts, decompression rate, and decompression path. Reverse modeling of a unique set of initial and decompression conditions to explain a natural sample is an obvious goal. Although determining a unique solution for a given natural sample is presently beyond the scope of SNGPlag, the model can be used to interrogate reasonable parameter space and generate a limited range of acceptable conditions, decompression rates, and paths.

Application of SNGPlag to natural systems

Several eruptions that have been the focus of previous research provide case studies to test the application of SNGPlag (Table 2). We discuss these eruptions in order of fastest-to-slowest decompression, which coincides with increasing complexity in possible decompression paths. Although the outputs of SNGPlag include microlite N_v, crystallinity, characteristic microlite size, and microlite CSD, most of the case studies do not provide all of those data; consequently, we may only compare our results with previously reported values. The final pressure chosen for SNGPlag model runs greatly affects the final results, as volatile pressure exerts a fundamental control on plagioclase crystallinity and thus the time evolution of supersaturation, $\Delta\phi$. In the eruptions discussed below, we use the same final pressures as the experimental studies to which we compare our model results (Chaitén, Ksudach, and Pinatubo), or we provide justification for the chosen pressure (Santa Maria and Mount St. Helens).

Chaitén, 2008

Chaitén volcano erupted in May 2008 in the southern Andes of Chile (Carn et al. 2009; Castro and Dingwell 2009). With only ~ 24 h precursor activity, the eruption distributed ~ 0.5 km^3 (DRE) of rhyolite tephra over southern Chile and Argentina (Alfano et al. 2011). The eruption produced a Plinian eruption column and numerous pyroclastic density currents, and formed a small caldera. The rhyolite pumice has < 1 vol% plagioclase phenocrysts (500–1000 µm in length). The rhyolitic groundmass contains sparse microlites or microphenocrysts (< 100 µm in length), suggesting that syneruptive decompression was fast enough to prevent microlite nucleation and growth. Castro and Dingwell (2009) used phase equilibria experiments to determine the magma which was likely stored at 120–200 MPa and 780–850 °C prior to eruption, with most likely conditions around ~ 825 °C and 150 MPa ($P_{total} = P_{H2O}$). They then used MSD decompression experiments, from 200 to 30 MPa at 780 °C and 150 to 30 MPa at 825 °C, to estimate a minimum decompression rate of ~ 40 MPa h^{-1}.

We reproduce those experimental decompression conditions using SNGPlag to calculate crystallinity and N_v using a continuous decompression path (Fig. 13). To replicate the natural phenocryst content, model runs contain tabular plagioclase crystals 500–1000 µm in size. These plagioclase are phenocrysts at 780 °C and 1 vol% antecrysts at 825 °C as

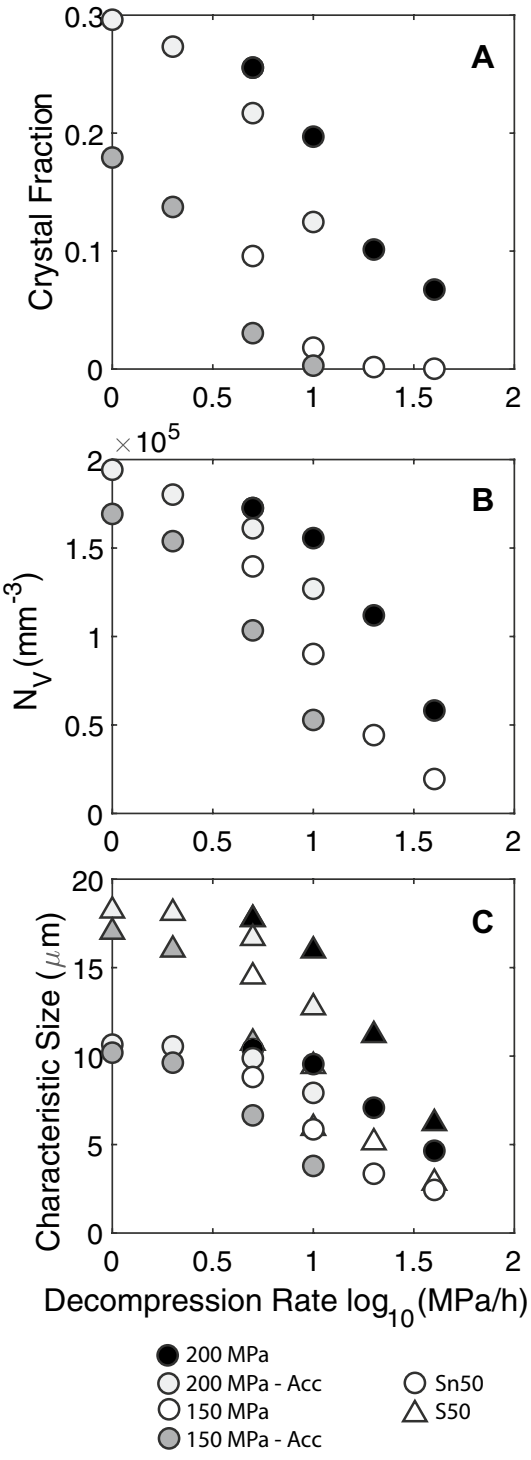

Fig. 13 SNGPlag simulations of Chaitén decompressions from 200 and 150 MPa to 30 MPa. **a** Final crystal fraction. **b** Final Nv. **c** Final Sn (triangles = 50 percentile; circles = equant method)

the latter starting conditions are just above the plagioclase liquidus. Simulations at 780 °C show systematic increases in crystallinity, N_v, and characteristic size with decreasing decompression rate (Fig. 13). The fastest decompression rate, 40 MPa h^{-1}, however, has a higher N_v than that reported by Castro and Dingwell. The series at 825 °C show a much lower degree of crystallization, with rates as slow as 10 MPa h^{-1} crystallizing < 2 vol% crystals with a characteristic size < 10 µm and $N_v < 9 \times 10^4$ mm^{-3}. If accelerating paths with final:initial rate ratios of 10 are used, then average rates as slow as 5 MPa h^{-1} result in crystallinities < 3 vol%, N_v of ~ 10^5 mm^{-3}, and characteristic sizes of ~ 13 µm. One possibility for higher calculated N_v, as compared to observed N_v, is that SNGPlag does not include an explicit nucleation delay (e.g., Couch et al. 2003; Brugger and Hammer 2010; Mollard et al. 2012). A nucleation delay of 2–12 h impinges on only a small portion of the decompression path for decompression rates slower than ~ 5 MPa h^{-1}, whereas decompression paths with a total duration comparable to the lag time may experience significant reduction in crystallization.

Santa Maria, 1902

The 1902 eruption of Santa Maria (Guatemala) distributed 8–20 km^3 of dacite tephra almost entirely as Plinian fall deposits (Rose 1972; Williams and Self 1983). The eruption is one of the largest Plinian eruptions to generate essentially no pyroclastic density currents. In addition, the > 8.5 km^3 DRE eruption is notable in that it did not generate a caldera, although the SW flank of Santa Maria did collapse in what may be an incipient caldera (Andrews 2014). The dacite pumice contains 15–20 vol% plagioclase phenocrysts, dominantly 70–100 µm in size, but with occasional phenocrysts > 200 µm. Andrews (2014) used phase equilibria experiments to determine that the likely pre-eruption storage conditions were 140–170 MPa and 840–850 °C, with plagioclase-hosted melt inclusions suggesting storage at ~ 170 MPa ($P_{total} = P_{H2O}$). Based on comparison of the observed microlite number densities (< 10^2 mm^{-3}) with decompression experiments on other magmas, Andrews (2014) suggested likely decompression rates of 18–36 MPa h^{-1}.

SNGPlag simulations for Santa Maria begin with an equilibrium crystallinity of 21 vol% and decompress via continuous linear and accelerating paths from 170 to 30 MPa at 845 °C (Fig. 14); P_{final} of 30 MPa is chosen as it agrees with that used in experimental decompression studies (Castro and Dingwell 2009; Andrews and Gardner 2010) and is similar to reasonable fragmentation depths (e.g., Rust and Cashman 2007; Gardner et al. 2017; Andrews et al. 2018). Microlite crystallinity increases systematically with decreasing decompression rate, from < 0.1 vol% at 40 MPa h^{-1} to ~ 1.8 vol% at 1 MPa h^{-1}. Rates as slow as

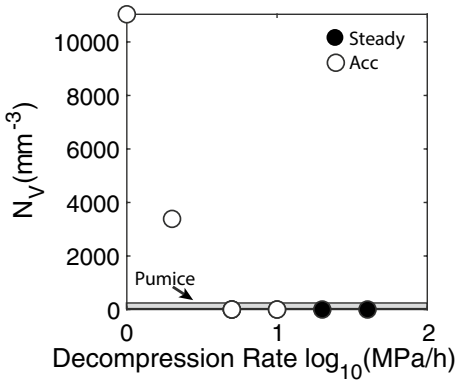

Fig. 14 Final N_v for steady and accelerating (Acc) decompressions of Santa Maria 1902 dacite

5 MPa h^{-1} produce no microlites larger than 1 µm, similar to the natural N_v. Runs at 2 and 1 MPa h^{-1} nucleate < 6×10^3 and < 1.4×10^4 mm^{-3} microlites, respectively. If accelerating rates with final:initial decompression ratios of 10 are used, then those average rates nucleate approximately half as many microlites. Interestingly, none of the model runs crystallize more than 1.3 vol% beyond the initial equilibrium phenocryst crystallinity, suggesting that bulk crystallinity is not particularly sensitive over the investigated range of decompression rates and paths. The minimum likely decompression rates suggested by SNGPlag, as slow as 5 MPa h^{-1}, are significantly slower than those predicted from comparison with previously published SSD and MSD decompression experiments. The most likely explanation for the much slower rates suggested by SNGPlag is that nucleation rates calculated from SSD and MSD experiments can be up to 20 times greater than the time-averaged instantaneous nucleation rates calculated for CD experiments (Befus and Andrews 2018), and thus, simple application of the former rates results in inflated estimates of decompression rate.

Ksudach KS1, 1800 ^{14}C yr BP

Ksudach volcano is a complex of nested calderas in southern Kamchatka (Braitseva et al. 1996). The most recent caldera-forming eruption, KS1, occurred ~ 1800 ^{14}C yr BP when ~ 8 km^3 rhyodacite (DRE) was erupted as Plinian falls and pyroclastic density currents (Braitseva et al. 1996; Andrews et al. 2007). The eruption deposits are distinguished by a shift from white to gray pumice approximately 70% through the eruption; about 35–50 h after the eruption began. The timing of the color change corresponds to caldera collapse and is the result of increased microlite content. The white and gray pumice contain ~ 10^2 and 2×10^6 mm^{-3} plagioclase microlites, respectively (Andrews et al. 2007; Andrews and Gardner 2010). The dominant microlite size in the gray pumice is ~ 2 µm, although we note that the

characteristic size, Sn, is coarser, around 5 µm. Insufficient plagioclase microlites occur in the White pumice for reliable determination of Sn. The pumice are otherwise compositionally indistinguishable, and contain ~ 3 vol% plagioclase phenocrysts ranging from 300 to 600 µm in size. Fe–Ti oxide thermobarometry, melt inclusion barometry, and phase equilibria experiments indicate pre-eruptive storage conditions of 100–125 MPa ($P_{total} = P_{H2O}$) and ~ 895 °C (Andrews et al. 2007; Andrews and Gardner 2010). Andrews and Gardner (2010) used multi-step decompression experiments (to final pressures of 20 MPa) to show that decompression slowed from > 36 to ~ 9 MPa h^{-1} following caldera collapse approximately 35–50 h into the eruption.

We performed SNGPlag simulations for different decompression paths from 100 to 20 MPa and 125 to 20 MPa at 895 °C (Fig. 15). Runs decompressed from 100 MPa with 300–600 µm phenocrysts do not crystallize for rates as slow as 10 MPa h^{-1}. If accelerating rates are used, then even an average rate of 5 MPa h^{-1} only nucleates ~ 600 mm^{-3} microlites > 1 µm in size. Simulations starting at 125 MPa show ≤ 1.5 vol% crystallization for rates as slow as 5 MPa h^{-1} (Fig. 15c, d). Those runs nucleate from 5×10^3 to 7.5×10^4 mm^{-3} crystals with characteristic sizes ranging from ~ 1 µm at 40 MPa h^{-1} to ~ 8 µm at 5 MPa h^{-1}. If accelerating rates are considered, we see that an average rate of 2 MPa h^{-1} results in < 4 vol% crystals with N_v of ~ 10^5 mm^{-3} and Sn of ~ 13 µm. We consider this rate to present a good estimate for the gray pumice, because it corresponds to a total decompression time of ~ 50 h, similar to the maximum estimate of time prior to eruption of the gray pumice and produces similar textures to those observed in the natural pumice.

To evaluate if the high plagioclase number densities in the gray pumice record a two-step decompression history, we consider SSD simulations from 125 MPa to a pause at 100 MPa or 75 MPa, and continuous decompressions with a pause at 100 MPa. These final pressures are chosen as a simplified representation of the pressure within the magma reservoir during caldera collapse prior to ascent and eruption of the gray pumice. We vary the SSD decompression rate to examine how many microlites are present prior to the final ascent following caldera collapse (Fig. 15e, f). None of the simulations are able to achieve N_v higher than ~ 1.6×10^5 mm^{-3}, even those held at 75 MPa with a pause for 500 h. SSD simulations with pauses more applicable to the KS1 eruption, 25 h, have N_v of ~ 3×10^4 mm^{-3}. Continuous decompressions with a 35 h pause at 100 MPa show an increase in Nv from ~ 6.6×10^4 mm^{-3} at 40 MPa h^{-1} to 1.7×10^5 mm^{-3} at 20 MPa h^{-1}, to 3.8×10^5 mm^{-3} at 10 MPa h^{-1}.

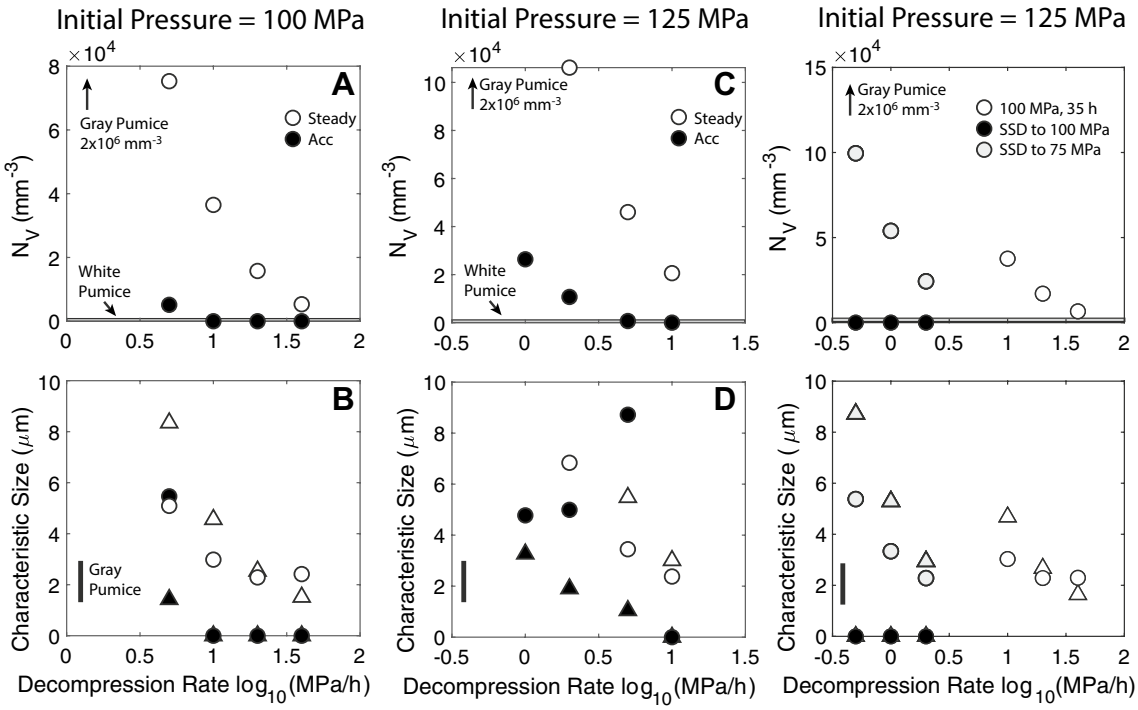

Fig. 15 SNGPlag simulations of Ksudach KS1 decompression. **a** N_v for steady and accelerating (Acc) decompression from 100 to 20 MPa. N_v for White pumice are indicated with the low box at the bottom of the panel; N_v for the gray pumice exceed the scale of the figure. **b** Sn for decompression from 100 to 20 MPa (triangles = 50 percentile; circles = equant method). **c** N_v for steady and accelerating (Acc) decompression from 125 to 20 MPa. **d** Sn for decompression from 125 to 20 MPa. **e** N_v for SSD and paused decompressions from 125 MPa. **f** Sn for SSD and paused decompressions from 125 MPa

The inability of SNGPlag to reproduce the high N_v observed in the gray pumice may indicate that the plagioclase nucleation and growth rates of the Ksudach rhyodacite at 895 °C differ from the Pinatubo dacite rates as measured at 780 °C (Befus and Andrews 2018); specifically, the Ksudach nucleation rate may be higher. The compositional and thermal dependence of nucleation and growth rates is supported by comparison of experimental studies showing that hotter, mafic magmas crystallize faster than cooler, silicic magmas (e.g., Hammer and Rutherford 2002; Couch et al. 2003; Szramek et al. 2006; Andrews and Gardner 2010); presumably, the nucleation and growth rates have similar functional forms with respect to $\Delta\phi$, but the absolute values of the rates shift upward with higher temperature or more mafic composition. Describing those dependences in the context of instantaneous nucleation and growth rates requires additional experimental work beyond the scope of this study. With those important caveats, SNGPlag can reproduce the pre- and syn-collapse White pumice textures with decompression as slow as 5 MPa h^{-1}; these rates are ~ 3–4 times slower than those indicated by MSD experiments (Andrews and Gardner 2010). If the nucleation rate is higher, then the decompression rate could be closer to that estimated by Andrews and Gardner (2010). Although SNGPlag cannot quantitatively determine the decompression rate recorded by the gray pumice textures, it does support the previous interpretation of much slower decompression following caldera collapse.

Mount Pinatubo, 1991

The 1991 caldera-forming eruption of Mount Pinatubo (Philippines) is the largest instrumented volcanic eruption. The eruption has been the focus of numerous experimental studies focusing on pre-eruptive storage conditions and decompression-induced crystallization (REFS). Indeed, Befus and Andrews (2018) used continuous decompression experiment on the Pinatubo dacite, from 220 to 30 MPa, to determine instantaneous nucleation and growth rates and thus develop the early version of SNGPlag. Here, we provide an abbreviated description of their results as applied to the Pinatubo dacite. Modeled decompression from 220 to 30 MPa at rates of 5–20 MPa h^{-1} produced reasonable agreement with the CSDs as measured by Hammer et al. (1999) for seven different pumice clasts; those rates overlap with those suggested by Browne and Szramek (2015) based on Hammer and Rutherford (2002) and Hammer et al. (1999). Befus and Andrews (2018) noted, however, that the steep slopes of the CSDs at small microlite size not recovered by steady decompression of the SNGPlag model could indicate unsteady decompression of some of the magma as suggested by Hammer et al. (1999).

Mount St Helens, 1980–1986

The 1980–1986 eruption of Mount St. Helens (U.S.A.) began with emplacement of a dacite cryptodome at shallow depth on the edifice's north flank; phreatic explosions on 27 March 1980 may mark the beginning of emplacement (Cashman 1988). At 0832 on 18 May 1980, the north flank collapsed, explosively decompressing the cryptodome and generating an explosive blast and pyroclastic density current (Lipman and Mullineaux 1981; Christiansen and Peterson 1981; Moore and Rice 1984; Hoblitt 2000). The dacite deposited in this event is referred to as the "blast dacite" and is primarily derived from the cryptodome. About 30 min later, the Plinian phase of eruption began, lasting until about 1730 that evening. During the Plinian event, about 1 km^3 of dacite tephra (~ 0.3 km^3 DRE) was deposited as pyroclastic flows, Plinian falls, and coignimbrite ash (Waitt and Dzurisin 1981; Criswell 1987; Carey et al. 1990; Andrews and Gardner 2009). Over the next 6 years, a series of dacite lava domes were emplaced and destroyed. Geophysical observations suggest that the St. Helens magma erupted from a storage region at 7–15 km depth (Scandone and Malone 1985). Melt inclusion barometry, phase equilibria experiments, and Fe–Ti oxide thermobarometry indicate pre-eruption storage at ~ 220 MPa ($P_{H2O} = 0.5–0.7\ P_{total}$) and 920–940 °C (Rutherford et al. 1985). Swanson et al. (1987) suggest that magma was stored in the conduit during the dome-building phases of eruption, and show that magma ascended from a depth of 2 km to the surface in a matter of hours prior to the May 1986 eruption. It should be noted that although the erupted tephra and lava have bulk dacite compositions, they are very crystal rich (~ 30–35 vol% plagioclase phenocrysts) and their glasses are rhyodacitic-to-rhyolitic in composition (Rutherford et al. 1985).

We apply SNGPlag to the Mount St. Helens dacite and compare the model results against measurements of microlite CSDs from the blast dacite as made by Cashman (1988). Conversion of those measured microlite CSDs to N_v provides an additional description of the equant (~ 10^4 mm^{-3}) and long axis (~ 2.7×10^4 mm^{-3}) N_v. We use the bulk dacite composition for sample SH-084 as reported by Rutherford et al. (1985) as a starting composition. At initial conditions of 154 MPa and 930 °C, MELTS predicts an equilibrium plagioclase phenocryst content of ~ 14 vol%, and thus, we add 16 vol% antecrysts to the runs to obtain the observed initial crystal fraction of 30 vol%. We find that SNGPlag recovers the observed CSDs and N_v with decompression rates as slow as ~ 2 MPa h^{-1}, provided the initial crystal sizes are 100 µm (Fig. 16). Slower rates, or runs using the characteristic crystal size of 1200 µm, produce too many crystals and CSDs that do not overlap the measured population (Fig. 16). These results highlight the importance of accurately specifying the size distributions of antecrysts and phenocrysts. We note that

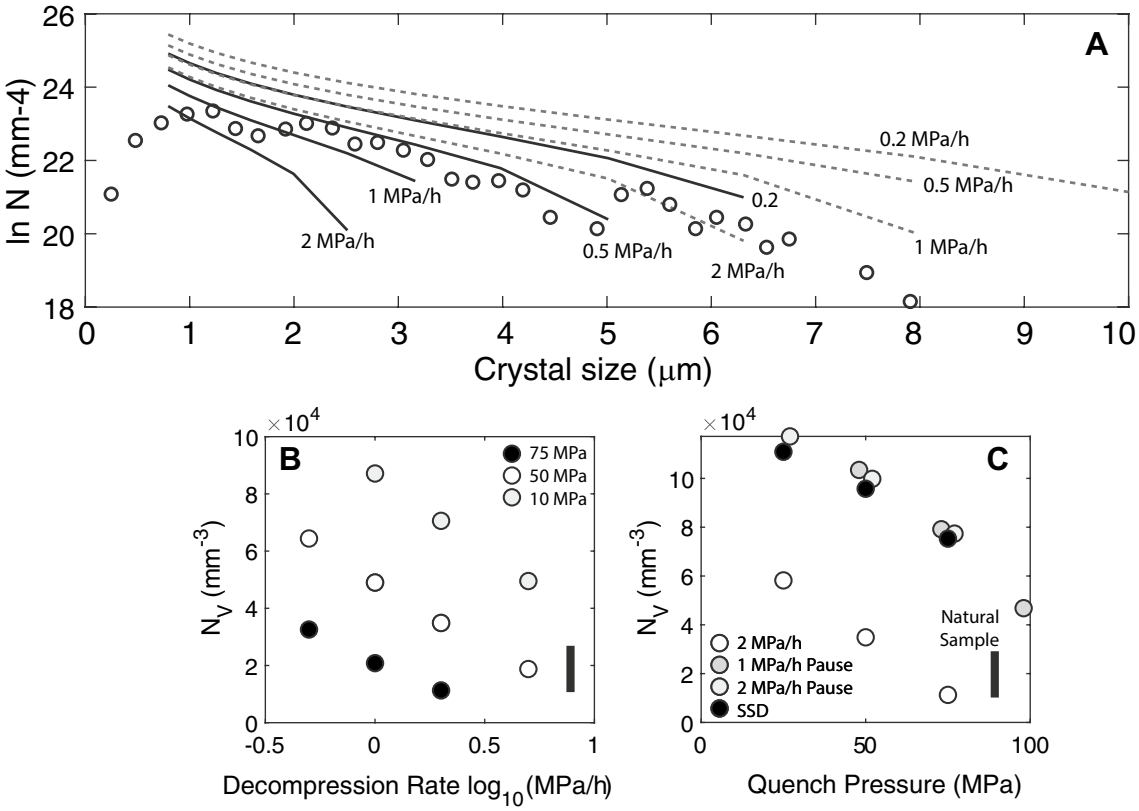

Fig. 16 **a** CSDs for decompression of Mount St. Helens cryptodome from 154 to 50 MPa with 100 mm antecryst and phenocrysts. Solid lines indicate runs quenched at 75 MPa and dashed lines indicate runs quenched at 50 MPa. Circles indicate long-axis CSDs as reported by Cashman (1988). **b** N_v for different quench pressures as a function of decompression rate. **c** N_v for decompressions from 154 to various quench pressures with different decompression paths (steady, pause of 720 h, and SSD to final pressure)

the best fits to the natural data occur with higher final pressures (50–100 MPa) than the likely emplacement pressure of the cryptodome (< 25 MPa; Donnadieu and Merle 2001) and surprisingly fast decompression rates. These discrepancies can be reconciled if we consider stalling of the magma at various depths, as proposed by Berlo et al. (2004), or that emplacement into the comparatively cool north flank of Mount St. Helens cooled portions of the dacite magma sufficiently to arrest further crystallization, or some combination of both mechanisms. The microlite textures reported by Cashman (1988) thus likely record a portion of the decompression interval, but not the entire time between the onset of decompression in March 1980 and eruption on 18 May 1980.

Conclusions

Supersaturation Nucleation and Growth of Plagioclase (SNGPlag) forward models the crystallization of plagioclase in response to isothermal decompression of magma. The model uses MELTS to determine the equilibrium volume fraction of plagioclase as a function of pressure and temperature for user-selected magma compositions (Gualda et al. 2012; Ghiorso and Gualda 2015). For any specified decompression path, the model calculates the difference between the equilibrium and calculated crystallinity for each time step to determine the supersaturation, which determines the instantaneous nucleation and growth rates at that time step. Inputs for SNGPlag include magma composition, initial and final pressure, temperature, decompression rate, decompression path (single-step, multi-step, continuous, accelerating, with or without pauses), and the presence or absence of antecrysts or phenocrysts. Outputs of SNGPlag include time series of crystallinity and supersaturation, CSDs, N_v, and total crystal surface area.

Microlite crystallization is strongly affected by the volume fraction and size distributions of antecrysts and phenocrysts, as well as decompression rate and path. In general, crystallinity and N_v increase and CSDs shift upward with decreasing decompression rate. At very slow rates, N_v and CSDs can shift downward as a smaller number of larger crystals nucleate and grow. Antecrysts and phenocrysts tend to reduce microlite crystallization, resulting in lower N_v and downward shifted CSDs, although bulk crystallinity may

be higher. These relationships are non-linear and dependent upon many factors, including the size distribution and shapes of pre-existing crystals. Finally, the details of a decompression path (e.g., single-step, multi-step, continuous, paused, accelerating) strongly affect microlite crystallization, such that different paths with the same average decompression rate can manifest very different crystal textures.

Comparison of SNGPlag simulations with previous experimental studies of decompression-induced crystallization of microlites shows that the model often predicts slower decompression rates than indicated by experimental studies. The most likely explanation for this disagreement is that the experimental studies were conducted using single- or multi-step decompression paths, which, for a given average decompression rate, produce higher microlite number densities and crystallinities than comparable continuous decompression paths. SNGPlag shows that estimates of syneruptive magma decompression and ascent rates based on single- and multi-step decompression may need to be reevaluated, and that instantaneous nucleation and growth rates (as well as potential nucleation delays) need to be experimentally determined over a broad range of magma compositions and temperatures.

Acknowledgements This research was funded by the Smithsonian Institution National Museum of Natural History. M. Ghiorso provided encouragement regarding the use of MELTS webservice. L. Waters contributed helpful comments that improved the SNGPlag program. Thoughtful comments by M. Ghiorso and two anonymous reviewers clarified and improved an earlier version of this manuscript.

References

Alfano F, Bonadonna C, Volentik ACM, Connor CB, Watt SBL, Pyle DM, Connor LJ (2011) Tephra stratigraphy and eruptive volume of the May, 2008, Chaitén eruption, Chile. Bull Volcanol 73:613–630

Andrews BJ (2014) Magmatic storage conditions, decompression rate, and incipient caldera collapse of the 1902 eruption of Santa Maria volcano, Guatemala. J Volcanol Geotherm Res 282:103–114

Andrews BJ, Gardner JE (2009) Turbulent dynamics of the 18 May 1980 Mount St. Helens eruption column. Geology 37:895–898

Andrews BJ, Gardner JE (2010) Effects of caldera collapse on conduit dimensions and magma decompression rate: an example from the 1800 14C yr BP eruption of Ksudach volcano, Kamchatka, Russia. J Volcanol Geotherm Res 198:205–216

Andrews BJ, Gardner JE, Tait S, Ponomareva VV, Melekestsev IV (2007) Dynamics of the 1800 14C yr BP caldera-forming eruption of Ksudach volcano, Kamchatka, Russia. In: Eichelberger J, Gordeev E, Kasahara M, Izbekov P, Lees J (eds) Volcanism and subduction: the Kamchatka region, vol 172. Geophysical Monograph, pp 325–342

Andrews BJ, Dufek J, Ponomareva VV (2018) Eruption dynamics and explosive-effusive transitions during the 1500 14C yBP eruption of Opala Volcano, Kamchatka, Russia. J Volcanol Geotherm Res 356:316–330

Befus KS, Andrews BJ (2018) Crystal nucleation and growth produced by continuous decompression of Pinatubo magma. Contrib Mineral Petrol 173:92. https://doi.org/10.1007/s00410-018-1519-5

Befus KS, Manga M, Gardner JE, Williams M (2015) Ascent and emplacement dynamics of obsidian lavas inferred from microlite textures. Bull Volcanol 77(10):1–17

Berlo K, Blundy J, Turner S, Cashman K, Hawkesworth C, Black S (2004) Geochemical precursors to volcanic activity at Mount St. Helens, USA. Science 306(5699):1167–1169. https://doi.org/10.1126/science.1103869

Braitseva OA, Melekestsev IV, Ponomareva VV, Kirianov VYu (1996) The caldera-forming eruption of Ksudach volcano about cal. A.D. 240: the greatest explosive event of our era in Kamchatka, Russia. J Volcanol Geotherm Res 70:49–65

Browne B, Gardner JE (2006) The influence of magma ascent path on the texture, mineralogy, and formation of hornblende reaction rims. Ear Planet Sci Lett 246:161–176

Browne B, Szramek L (2015) Rates of magma ascent and storage. In: Sigurdsson H, Houghton B, McNutt S, Rymer H, Stix J (eds) Encyclopedia of volcanoes, 2nd edn. Academic Press, London, pp 203–214

Brugger CR, Hammer JE (2010) Crystal size distribution analysis of plagioclase in experimentally decompressed hydrous rhyodacite magma. Earth Planet Sci Lett 300(3):246–254

Burgisser A, Gardner JE (2005) Experimental constraints on degassing and permeability in volcanic conduit flow. Bull Volcanol 67:42–56. https://doi.org/10.1007/s00445-004-0356-8

Carey S, Sigurdsson H, Gardner JE, Criswell W (1990) Variations in column height and magma discharge during the May 18, 1980 eruption of Mount St. Helens. J Volcanol Geotherm Res 43:99–112

Carn SA, Pallister JS, Lara L, Ewert JW, Watt S, Prata AJ, Thomas RJ, Villarosa G (2009) The unexpected awakening of Chaiten Volcano, Chile. EOS Trans AGU 90:205–206

Cashman KV (1988) Crystallization of Mount St. Helens 1980–1986 dacite: a quantitative textural approach. Bull Volcanol 50:194–209

Cashman KV, Marsh B (1988) Crystal size distribution (CSD) in rocks and the kinetics and dynamics of crystallization II: Makaopuhi lava lake. Contrib Mineral Petrol 99:292–305

Castro JM, Dingwell DB (2009) Rapid ascent of rhyolitic magma at Chaitén volcano, Chile. Nature 461(7265):780

Christiansen RL, Peterson DW (1981) Chronology of the 1980 eruptive activity. In: Lipman PW, Mullineaux DR (eds) The 1980 eruptions of Mount St. Helens, Washington, vol 1250. US Geol Surv Prof Pap, pp 17–30

Coombs ML, Vazquez JA (2014) Cogenetic late Pleistocene rhyolite and cumulate diorites from Augustine volcano revealed by SIMS ^{238}U–^{230}Th dating of zircon, and implications for silicic magma generation by extraction from mush. Geochem Geophys Geosys 15:4846–4865. https://doi.org/10.1002/2014GC005589

Coombs ML, Eichelberger JC, Rutherford MJ (2002) Experimental and textural constraints on mafic enclave formation in volcanic rocks. J Volcanol Geotherm Res 119:125–144

Couch S, Sparks R, Carroll M (2003) The kinetics of degassing-induced crystallization at Soufriere hills volcano. Montserrat J Petrol 44(8):1477–1502

Criswell CW (1987) Chronology and pyroclastic stratigraphy of the May 18, 1980, eruption of Mount St. Helens. J Geophys Res 92:10237–10266

Devine JD, Rutherford MJ, Gardner JE (1997) Petrologic determination of ascent rates for the 1995–1997 Soufriere hills volcano andesitic magma. Geophys Res Lett 25:3673–3676

Donnadieu F, Merle O (2001) Geometrical constraints of the 1980 Mount St. Helens intrusion from analogue models. Geophys Res Lett 28:639–642

Eaton JP, Richter DH, Krivoy HL (1987) Cycling of magma between the summit reservoir and Kilauea Iki lava lake during the 1959 eruption of Kilauea volcano. USGS Prof Pap 1350:1307–1335

Eichelberger JC, Carrigan CR, Westrich HR, Price RH (1986) Non-explosive silicic volcanism. Nature 323:598–602

Ferguson DJ, Gonnermann HM, Ruprecht P, Plank T, Hauri EH, Houghton BF, Swanson DA (2016) Magma decompression rates during explosive eruptions of Kilauea volcano, Hawaii, recorded by melt embayments. Bull Volcanol 78:71

Gardner JE, Llewellin EW, Watkins JM, Befus KS (2017) Formation of obsidian pyroclasts by sintering of ash particles in the volcanic conduit. Earth Planet Sci Lett 459:252–263

Geschwind C-H, Rutherford MJ (1995) Crystallization of microlites during magma ascent: the fluid mechanics of 1980–1986 eruptions at Mount St Helens. Bull Volcanol 57(5):356–370

Ghiorso MS, Gualda GAR (2015) An H2O-CO2 mixed fluid saturation model compatible with rhyolite-MELTS. Contrib Mineral Petrol 169:53

Gualda GAR, Ghiorso MS, Lemons RV, Carley TL (2012) Rhyolite-MELTS: A modified calibration of MELTS optimized for silica-rich, fluid-bearing magmatic systems. J Petrol 53:875–890

Hammer JE (2004) Crystal nucleation in hydrous rhyolite: experimental data applied to classical theory. Am Mineral 89(11–12):1673–1679

Hammer JE, Rutherford MJ (2002) An experimental study of the kinetics of decompression-induced crystallization in silicic melt. J Geophys Res 107(B1):ECV-8-1. https://doi.org/10.1029/2001JB000281

Hammer J, Cashman K, Hoblitt R, Newman S (1999) Degassing and microlite crystallization during pre-climactic events of the 1991 eruption of Mt. Pinatubo, Philippines. Bull Volcanol 60(5):355–380

Harlow DH, Power JA, Laguerta EP, Ambubuyog G, White RA, Hoblitt RP (1996) Precursory seismicity and forecasting of the Jun 15, 1991, eruption of Mount Pinatubo. In: Newhall C, Punongbayan RS (eds) Fire and mud: eruptions and lahars of Mount Pinatubo, Phlilippines, pp 285–306

Hoblitt RP (2000) Was the 18 May 1980 lateral blast at Mt St Helens the product of two explosions? Philos Trans R Soc Lond A358:1639–1661

Humphreys MC, Menand T, Blundy JD, Klimm K (2008) Magma ascent rates in explosive eruptions: constraints from H_2O diffusion in melt inclusions. Earth Planet Sci Lett 270(1):25–40

Jaupart C, Allegre C (1991) Gas content, eruption rate and instabilities of eruption regime in silicic volcanoes. Earth Planet Sci Lett 102:413–429

Lipman PW, Mullineaux DR (eds) (1981) The 1980 eruptions of Mount St. Helens, Washington. US Geol Surv Prof Pap 1250:844

Liu Y, Anderson AT, Wilson CJN (2007) Melt pockets in phenocrysts and decompression rates of silicic magmas before fragmentation. J Geophys Res 112:B06204

Lloyd AS, Ruprecht P, Hauri EH, Rose W, Gonnermann H, Plank T (2014) NanoSIMS results during explosive basaltic eruptions. J Volcanol Geotherm Res 283(1):1–18

Marsh B (1988) Crystal size distribution (CSD) in rocks and the kinetics and dynamics of crystallization I: theory. Contrib Mineral Petrol 99:277–291

Martel C (2012) Eruption dynamics inferred from microlite crystallization experiments: application to Plinian and dome-forming eruptions of Mt. Pelée (Martinique, Lesser Antilles). J Petrol 53(4):699–725

Martel C, Schmidt BC (2003) Decompression experiments as an insight into ascent rates of silicic magmas. Contrib Mineral Petrol 144(4):397–415

Mollard E, Martel C, Bourdier J-L (2012) Decompression-induced crystallization in hydrated silica-rich melts: empirical models of experimental plagioclase nucleation and growth kinetics. J Petrol 53(8):1743–1766

Moore JG, Rice C (1984) Chronology and character of the May 18, 1980 explosive eruption of Mount St. Helens. In: Explosive volcanism: inception, evolution and hazards. National Academies of Sciences, Washington, pp 133–142

Moussallam Y, Rose-Koga EF, Koga KT, Médard E, Bani P, Devidal JL, Tari D (2019) Fast ascent rate during the 2017–2018 Plinian eruption of Ambae (Aoba) volcano: a petrological investigation. Contrib Mineral Petrol 174(11):90

Mujin M, Nakamura M, Aa M (2017) Eruption style and crystal size distributions: crystallization of groundmass nanolites in the 2011 Shinmoedake eruption. Am Mineral 102:2367–2380

Myers ML, Wallace PJ, Wilson CJN, Morter BK, Swallow EJ (2016) Prolonged ascent and episodic venting of discrete magma batches at the onset of the Huckleberry Ridge supereruption, Yellowstone. Earth Planet Sci Lett 451:285–297

Myers ML, Wallace PJ, Wilson CJN, Watkins JM, Liu Y (2018) Ascent rates of rhyolitic magma at the onset of caldera-forming eruptions. Am Mineral 103(6):952–965

Nabelek PI, Taylor LA, Lofgren GE (1978) Nucleation and growth of plagioclase and the development of textures in a high-alumina basaltic melt. Proc Lunar Planet Sci Conf 9:725–741

National Academies of Sciences, Engineering, and Medicine (2017) Volcanic eruptions and their repose, unrest, precursors, and timing. The National Academies Press, Washington. https://doi.org/10.17226/24650

Power JA, Murray TL, Marso JN, Laguerta EP (1996) Preliminary observations of seismicity at Mount Pinatubo by use of the seismic spectral amplitude measurement (SSAM) system, May 13–June 18 1991. In: Newhall C, Punongbayan RS (eds) Fire and mud: eruptions and lahars of Mount Pinatubo, Phlilippines, pp 269–284

Roman DC, Cashman KV, Gardner CA, Wallace PJ, Donovan JJ (2006) Storage and interaction of compositionally heterogeneous magmas from the 1986 eruption of Augustine volcano, Alaska. Bull Volcanol 68:240–254

Rose WI (1972) Notes on the 1902 eruption of Santa Maria volcano, Guatemala. Bull Volcanol 36:29–45

Rust AC, Cashman KV (2007) Multiple origins of obsidian pyroclasts and implications for changes in dynamics of the 1300 B.P. eruption of Newberry volcano, USA. Bull Volcanol 69:825–845

Rutherford MJ, Hill PM (1993) Magma ascent rates from amphibole breakdown: an experimental study applied to the 1980–1986 Mount St. Helens eruptions. J Geophys Res 98(B11):19667–19685

Rutherford MJ, Sigurdsson H, Carey S, Davis A (1985) The May 18, 1980, eruption of Mount St. Helens 1. Melt composition and experimental phase equilibria. J Geophys Res 90:2929–2947

Scandone R, Malone SD (1985) Magma supply, magma discharge and readjustment of the feeding system of Mount St. Helens during 1980. J Volcanol Geotherm Res 23:239–262

Shea T, Hammer JE (2013) Kinetics of cooling-and decompression-induced crystallization in hydrous mafic-intermediate magmas. J Volcanol Geotherm Res 260:127–145

Suzuki Y, Fujii T (2010) Effect of syneruptive decompression path on shifting intensity in basaltic sub-Plinian eruption: Implication of microlites in Yufune-2 scoria from Fuji volcano, Japan. J Volcanol Geotherm Res 198:158–176

Suzuki Y, Gardner JE, Larsen JF (2007) Experimental constraints on syneruptive magma ascent related to the phreatomagmatic phase of the 2000 AD eruption of Usu volcano, Japan. Bull Volcanol 69:423–444

Swanson DA, Dzurisin D, Holcomb RT, Iwatsubo IY, Chadwick WW, Casadevall TJ, Ewert JW, Heliker CC (1987) Growth of the lava dome at Mount St. Helens, Washington (US), 1981–1983. Spec Pap Geol Soc Am 212:1–16

Szramek L, Gardner JE, Larsen JF (2006) Degassing and microlite crystallization of basaltic andesite magma erupting at Arenal volcano, Costa Rica. J Volcanol Geotherm Res 157:182–201

Toramaru A (2006) BND (bubble number density) decompression rate meter for explosive volcanic eruptions. J Volcanol Geotherm Res 154:303–316

Toramaru A, Noguchi S, Oyoshihara S, Tsune A (2008) MND (microlite number density) water exsolution rate meter. J Volcanol Geotherm Res 175(1–2):156–167. https://doi.org/10.1016/j.jvolgeores.2008.03.035

Turnbull D (1948) Transient nucleation. Trans Met Soc 175:774–783

Waitt RB Jr, Dzurisin D (1981) Proximal air–fall deposits fmor the May 18 eruption—stratigraphy and field sedimentology. In: Lipman PW, Mullineaux DR (eds) The 1980 eruptions of Mount St. Helens, Washington, vol 1250. US Geol Surv Prof Pap, pp 601–616

Waters LE, Andrews BJ, Lange RA (2015) Rapid crystallization of plagioclase phenocrysts in silicic melts during fluid-saturated ascent: phase equilibrium and decompression experiments. J Petrol 56(5):981–1006. https://doi.org/10.1093/petrology/egv025

Williams SN, Self S (1983) The October 1902 Plinian eruption of Santa Maria volcano, Guatemala. J Volcanol Geotherm Res 16:33–56

Yoshida S, Koyaguchi T (1999) A new regime of volcanic eruption due to the relative motion between liquid and gas. J Volcanol Geotherm Res 89:303–315